COMBUSTION OF POLYMERS IN A LOW PRESSURE AND LOW OXYGEN ENVIRONMENT

by

MARIUSZ ZARZECKI

A Thesis submitted to the

Graduate School-New Brunswick

Rutgers, The State University of New Jersey

In partial fulfillment of the requirements

For the degree of

Master of Science

Graduate Program in Mechanical & Aerospace Engineering

Written under the directions of

Professor Francisco Javier Diez

and

Professor Tobias Rossmann

and approved by

_____

_____

_____

New Brunswick, New Jersey

May 2012

ABSTRACT OF THE THESIS

COMBUSTION OF POLYMERS IN A LOW PRESSURE AND LOW OXYGEN ENVIRONMENT

By MARIUSZ ZARZECKI

Thesis Director:

Professors Francisco Javier Diez and Tobias Rossmann

The effect of low pressure on the behavior of fires is very important to the study of fire safety in the aviation industry. This thesis explores the effect of low pressure on different components of flammability at low pressures, like those encountered at high altitude. An experiment was setup to measure the time to ignition, the mass flux at ignition, as well as the steady burning mass flux for different pressures and oxygen concentrations. The test measured the mass loss, oxygen consumption, soot production and average flame temperature. A square sample of PMMA was burned under different external heat fluxes, total pressures and oxygen concentrations. The experiments were compared to analytical expressions, to try to understand how pressure and oxygen concentration affect the behavior of a fire. Low pressure environment reduced

the ignition delay time, indicating a sample is more prone to ignition at lower pressure. On the other hand the sample showed a reduction of steady burning mass flux, indicating the fire is less intense at lower pressure. The results show a good agreement with the analytical analysis

Acknowledgments

I would like to thank Profs. Diez and Rossmann,for their guidance and support during my work to complete this thesis. I would like to thank Dr. Richard Lyon at the FAA for giving me the opportunity to work on this project, and for his support and insight into the fundamentals of fire safety science. I would like to thank Prof. Quintiere for his time to help me understand the fundamentals of solid combustion and his combustion model that was a major part of this thesis.

I would like to thank Mr. Richard Hill and Mr. Gus Sarkos at the Fire Safety Branch of the Federal Aviation Administration's for providing the funding and the facilities for me to be able to conduct my research. Their knowledge of aviation fires safety regulations helped me understand the motivations for the purpose of this research.

I would like to thank Mr. Richard Walters, Mr. Sean Crowley and Mr. Dave Mills for their help in developing the setup, and helping me obtain the needed materials. I would also like to thank the entire staff at the of the Fire Safety Branch of the Federal Aviation Administration's William for their help in the completion of this thesis.

Table of Contents

List of Figures

Chapter 1

Introduction

1.1 Motivation

For the most part of our daily lives the effect of atmospheric pressure is largely irrelevant; hence we take it for granted that the pressure stays constant. As such the majority of the fire tests, and the regulation that are based on those tests are usually limited to the standard atmospheric pressure of 1 atm (101.3 kPa). The atmospheric pressure is not constant though, once you move above or below the sea level.

The relation for pressure versus altitude can be simply derived from the fact that at a hydrostatic equilibrium the change in pressure over an infinitesimal change in altitude, must be balanced by the gravitational force acting on it. This can be represented as a differential equation of the form:

$$\frac{dP}{dz} = -\rho g \tag{1.1}$$

where P is the pressure, ρ is the air density, g is the gravitational acceleration, and z is the altitude. From an ideal gas law the relation is

$$P = \rho RT \tag{1.2}$$

where T is the temperature and R is the gas constant. Substituting Eq. 1.1 into Eq. 1.2 and solving for pressure gives:

$$P = P_0 \exp\left(-\frac{gh}{RT}\right) \quad (1.3)$$

where h is the altitude and P_0 is the pressure at the sea level. Substituting 15 º C (288 K) for T, 101.3 kPa for P_0, and 286.9 J/kg for R, gives the pressure at a given altitude. The resulting values for the variation of pressure with altitude are shown in Fig. 1.1.

There are several cities around the world with populations of more than 600,000 that are located one mile above sea level and higher. Denver (USA), with an altitude of 1 mile (1609 m) has an atmospheric pressure of 0.83 atm, La Paz (Bolivia), has an altitude of 3,697 m and pressure of 0.64 atm, and Mexico City, located 2237 m above sea level with the atmospheric pressure of 0.76 atm [1].

Another condition where material might encounter low pressure environment is in an airplane. Several regulatory authorities performed fire test that showed that a hidden fire left unattended could become uncontrollable within 8-10 minutes [2]. The same studies have shown that the crew only had 15-20 minutes to land the airplane, before catastrophic damage occurred [2]. National transportation safety board commissioned FAA to investigate fire suppression systems in cargo airplanes. This was after a February 7, 2006 accident, when a UPS McDonnell Douglas airplane had to perform emergency landing after smoke was detected in the cabin [3]. Currently the FAA-accepted method for controlling

fires on cargo airplanes is to turn off the ventilation and then depressurize the cargo hold. The effect of pressure on fires is not well understood, and given that fires can occur at any altitude the effect of pressure should not be neglected.

1.2 Background

Tewarson (2000) investigated the effect of increased pressure and oxygen concentration on the flame heat flux [4]. An increase in flame heat flux is proportional to the mass loss, and hence it's a good representation of the intensity of the fire. He concluded that the pressure plays a more important role in fires compared with oxygen concentration. He ran tests for pressures ranging from 1 to 38 atm and saw a tenfold increase in the flame heat flux. At 35 % of oxygen the heat flux reached a peak value, and hence no further increase in flame heat flux was observed. Frey and T'ien (1976) showed how the flame spread rate is reduced with pressure, but the pressure dependence decreased with an increase in molar fraction of oxygen [5].

Test performed on flame spread were performed by McAlevy and MaGee (1969) [6]. Their tests showed that the flame speed is controlled by a gas phase physical process of heat and mass transfer, and specifically it is a function of molar fraction of oxygen and pressure. Their relation relates pressure P and molar fraction of oxygen Y_{ox}^{m} to flame spread velocity V and is given by:

$$V \propto \left(P Y_{ox}^{m}\right)^{\phi} \tag{1.1}$$

where m, and ϕ are constants. McAlevy and MaGee (1965) determined m and ϕ to be 3 and .82 respectively, suggesting that the velocity decreased with pressure and similarly with a decrease in oxygen concentration, but at a much higher rate for the latter. Therefore the effect of oxygen concentration plays a much larger role. West (1997) studied the effect of oxygen enrichment in reduced pressure environments [7]. West showed a decrease in the burning rate of paper and clothing at higher altitudes, but if the partial pressure was maintained constant as the altitude increased the burning rate increased. This again suggests that the oxygen plays a more important role in the burning behavior of flammable materials.

Nakaura *et al.* (2009) investigated the flame spread on electrical wires in reduced pressure environments [8]. His findings are contradictory to those by McAlevy and West (1965), where the pressure reduced flame spread. He tested NiCr and Fe wires coated in polyethylene and pressures ranging from 20 to 101 kPa. The tests showed that the flame spread increased as the pressure was lowered for the NiCr wire, but stayed relatively constant for the Fe wire. Nakamura noticed the flame became shorter and wider at lower pressure, causing it to wrap around the wire. Nakamura surmised that, since the surface area of the wire exposed to the flame increased, that the net heat transfer back to the sample was larger.

There is very limited amount of research done on the formation of soot at low pressure and oxygen concentration. Studies done at pressures above atmospheric (Roditcheva and Bai (1997)) suggest an increase in soot formation

with an increase in total pressure [9]. This phenomenon is thought to occur due to an increase in density and hence increase in soot precursor species concentration, resulting in an increase in a soot surface growth rate. Another consideration involves the increase in the residence time, with increase in pressure, of soot precursors in the hotter portion of the flame resulting in the relatively slow soot formation chemistry to take effect and form more soot particles. The production of soot in flame contributes to an increase in flame heat flux through the re-radiation of energy from the soot particles back to the burning sample. Beltrame *et al.* (2001) noticed a 400% increase in soot production when increasing oxygen concentration by 21 to 30% oxygen concentration for methane flames showing that soot production is proportional to oxygen concentration, but Tewarson (1981) shows that the effect of oxygen on soot production is dependent on the material being burned [10][11].

Ignition studies at reduced pressure have been performed by McAllister *et al.* (2010) and showed a decrease in time to ignition with reduced pressure [12]. She concluded that as the pressure is decreased the convective heat losses were also decreased, and hence allowing the material to reach the ignition temperature faster. The results showed a u-shape dependence of ignition time with pressure. At higher pressure the convective heat loss played a dominant role, but as the pressure reduced the chemical kinetic effects became important and the time to ignition started to decrease with further decrease in pressure. The ignition results suggest that since the flame spread rate is inversely related to time to ignition, i.e. the flame spread rate should increase with a decrease in

pressure. This could be due to the increase in flame stand-off distance resulting in lower heat flux from the flame [13].

1.3 Objective

The purpose of this thesis is to obtain burning rate measurements for PMMA at different pressure, in order to be able to predict the behavior of fires in low pressure environments. Since fires can occur in low pressure environments a fundamental understanding of the physical processes controlling their behavior needs to be researched. An analytical approach will be used to model the different components controlling the fires and is compared to the experimental results. The tests were done in a vacuum chamber at reduced pressure to simulate high altitude conditions. The theoretical analysis will allow for a deeper understanding of the physics involved in the burning process, and how pressure affects them.

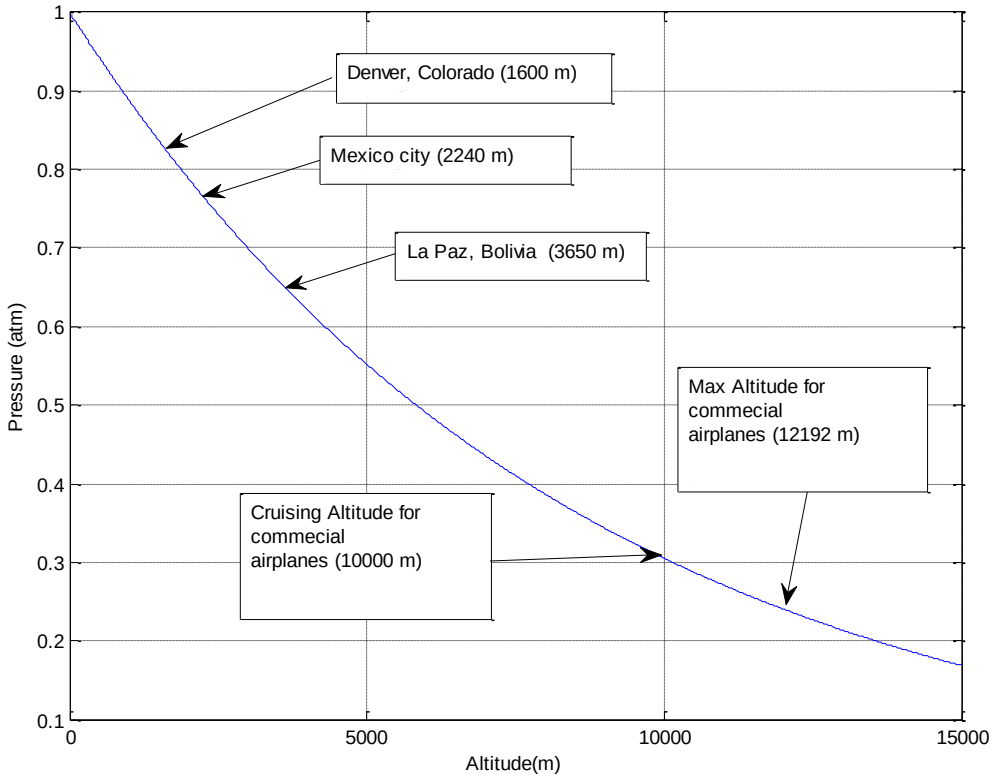

Figure 1.1 Pressure variation at different altitudes.

Chapter 2

Experimental Setup and Procedure

All experiments were performed under the supervision of the Federal Aviation Administration's research and development group for fire safety. The FAA pressure modeling facility is located at the William J. Hughes Technical Center within the Atlantic City airport, New Jersey. The tests were performed with a mass loss calorimeter that was placed inside a 10 cubic meter pressure vessel shown in Fig. 2.1. The tests were designed to measure the mass loss, and oxygen consumption, during steady burning of PMMA samples at pressures ranging from 0.18 atm to 1 atm. The samples in these tests were exposed to external heat fluxes, anywhere from 10 to 75 kW/m^2. The tests where repeated for oxygen concentrations between 12 to 21 %, but only for external heat flux of 16 kW/m^2. Soot yield and flame temperature measurements were taken at three different heat fluxes, where the only variable was the pressure.

2.1 Pressure modeling facility

The pressure vessel has the capability to simulate pressures up to 48,000 feet and maintain a flow through rate of 7 liters per second (lps). The system is connected to an air supply system and the flow rate can be adjusted to a specified setting. All the tests had been performed with a flow rate of 7 lps corresponding to a minimum flow rate required to maintain oxygen consumption within the control volume below 10%. The mass loss calorimeter was then placed

inside a 1 cubic meter container within the pressure vessel where the local oxygen concentration could be varied. The airflow enters through the bottom of the container via a ½ inch pipe perforated every 1 cm. The air exits through the top of the container via a 3 inch pipe, expelling the exhaust gas into the inside of the pressure vessel. The air is then removed via a vacuum pump to the outside. The air within the container is maintained at a specified oxygen concentration. The container is open to the inside of the pressure vessel at the exhaust port. The nitrogen was produced using a Floxal nitrogen generation system manufactured by Air Liquide. The nitrogen was mixed with the house air to produce gas mixtures with oxygen concentrations below 21 %.

All tests were monitored via a closed circuit TV system, and recorded with a commercial FS100 Canon camera.

2.2 Mass loss calorimeter

The main instrument used to measure the mass loss during flaming combustion was the mass loss calorimeter (Fig. 2.2). The calorimeter consists of a balance, a cone shaped heater, a shutter, and a spark igniter. The balance is connected to a PC were the mass as a function of time can be stored for the duration of the test. The balance is capable of measuring weights to within 10 milligrams. The cone heater, located 10 cm above the sample surface, can generate heat fluxes up to 75 kW/m^2. While the heater is ramped up there is a shutter separating it from the sample to prevent the sample from heating up before the test begins. When the test begins the shutters opens and the igniter is placed 13 mm above the surface as per ASTM E 1354 standard [14]. Both the

shutter and the igniter are triggered remotely. All the data was captured using custom software part of the MLC. The software and hardware were manufactured by Govemark.

2.2.1 Mass loss

One of the most effective ways to measure the intensity of a fire is to monitor the amount of fuel being consumed, as a larger fire needs more fuel to sustain itself. Since mass loss is proportional to the amount of energy released, a mass loss measurement will provide insight into the strength of the fire.

A load cell, placed under the flaming sample continuously monitors the mass as a function of time. The balance was accurate to within 10 milligrams. The balance was calibrated using the sample holder to access the zero value for mass, and a 454 gram mass for the secondary point. The line than can be then drawn from those two points to give a correlation between the voltage and mass.

An example of a single test can be seen in Fig. 2.3. The data is characterized by an initial, small decrease in sample mass, followed by a sudden jump at the onset of flaming ignition. Following the onset of ignition the sample reaches steady state burning represented by a constant slope line. Once the sample runs out of fuel, or can produce a critical mass flux, the flame goes out and the test is over.

2.2.2 Mass loss rate

Since the mass flux is the most relevant value for the purpose of fire research, the numerical derivative of the mass loss data was needed. The

derivative was calculated using a 5 point central difference scheme, as recommended by ASTM E-1354 [14]. The data was further smoothed using a linear, 21-point Savitzky-Golay filter in Matlab. The data, before and after smoothing, can be seen in Figs. 2.4 and 2.5, respectively.

The mass loss rate data is characterized by a sudden jump at ignition, followed by steady burning. When the heat finally reaches the insulation at the back of the sample there is a sudden jump in mass loss rate, followed by a sudden decrease. When the flame reaches the insulation at the back of the sample, it allows for more energy to be transferred to vaporizing the fuel, thereby temporarily increase the mass loss rate. For the purpose of this study the mass loss rate of interest occurs right before the ignition, termed critical mass flux at ignition, and the steady burning mass loss rate.

2.2.3 Oxygen consumption calorimeter system

The mass loss calorimeter was placed inside a closed container (Figure 2.6), inside the vacuum chamber, so that the amount of oxygen consumed by the fire can be measured. This allows for the heat release rate to be calculated, giving an indication of the intensity of the fire. A sample tube was placed in the exhaust, which extracted an air sample. The 3.175 mm tubing was made of copper for the first 2 m, and vinyl for the other 3 m. The sampled air was then brought up to ambient pressure via a Heathrow Scientific vacuum pump. A Teledyne cell B1 oxygen sensor measured the oxygen partial pressure, giving a relative amount of oxygen being consumed. The sensor was wired to an amplifier where the signal strength was stepped up, increasing the signal to noise ratio. A LabVIEW data

acquisition system was used to collect the data. A LabVIEW calibration file was written to convert voltage to the corresponding oxygen concentration. The calibration was done using two points, which were then fitted with a line. One point was at zero, corresponding to zero oxygen concentration, and the other was at ambient concentration. A program was written in Labview allowing for the data to be recorded and stores in text files. The flow-through rate was kept constant at 15 cfm (7 liters per second).

A Whatman grade epm 2000 paper filter was used for the tests. It achieves particle retention rate of 98% for particles larger than 2 μm. The filter was placed in-line with the sampling tube for the duration of the test. The change in mass of filter before and after the test gave a relative soot production between tests for different pressures.

2.2.4 Heat release rate

Another way to characterize the magnitude of a fire is using an oxygen consumption calorimetry. The basic principle originates from Thornton (1917) [15]. He discovered that for a complete combustion there is a constant amount of heat release per unit mass of oxygen consumed. Huggett(1980) extended the theory to organic solids and showed that the heat released per unit mass of oxygen is about 13.1 MJ kg^{-1} [16]. Given that the value of 13.1 is obtained from complete combustion, according to Babrauskas (1992) it can be used in practical application to within

+- 5% [17].

An example of an actual test can be seen in Fig. 2.7. Once the oxygen consumpiton is known the heat realease rate can be obtained from Eq. 2.1 [17].

$$\dot{q} = E[\frac{Y_{O_2}^{A^0} - Y_{O_2}^{A}}{1 - Y_{O_2}^{A}}] * \dot{m}_a \frac{M_{O_2}}{M_{air}} \qquad (2.1)$$

where $\dot{q}$ = Rate of heat release (kW), E = Heat released per O_2 consumed (13.1 MJ-kg^{-1} of O_2), M_{air} = Molecular weight of the incoming air (kg kmol^{-1}), M_{O_2} = Molecular weight of oxygen (kg kmol^{-1}), $\dot{m}_a$ = Mass flow rate of the incoming air (kg s^{-1}), $Y_{O_2}^{A^0}$ = Mole fraction of incoming oxygen and $Y_{O_2}^{A}$ = Mole fraction of oxygen at the exit. The output form Eq. 2.1 can be seen in Fig. 2.8. The results were smoothed using a Savitzky-Golay filter in matlab.

2.3 Sample preparation

The test was designed to measure a 1-D burning rate for 10 cm x 10 cm sample of PMMA (Plexiglass-G). The sample is placed 10 cm below the cone heater, which has been set beforehand to a specific heat flux using a Gardon gauge. The sample material was then wrapped in an aluminum foil, in the hope of preventing the material from dripping out, while leaving the top surface exposed. A 2 inch layer of Kaowool material was placed in the back of the sample to minimize heat losses. The procedure for sample preparation can be seen in Fig. 2.9.

2.4 Experimental Procedure

Two separate programs were used to obtain the mass loss and oxygen consumption data. A program was written in Labview to collect and save the oxygen consumption data. The sampling rate was 500 data points per second. The mass loss data was collected using the data acquisition written by Govmark that came with the hardware.

Once the sample was placed on the balance, the container holding the mass loss calorimeter was closed followed by the entire pressure vessel. The soot filter was weighted and then placed before the sampling pump. The pressure inside the vessel was manipulated using a flow controller located before the vacuum pump. Once the desired pressure was set the pump was turned on. It took 5-10 minutes for the pressure to reach the desired setting, depending on the strength of the vacuum required. The cone heater and the air supply were turned on at about the same time. Once the system reached steady state, which usually

happened within 10 minutes of the whole system being turned on, the data acquisition system began capturing data. When the shutter opened the spark igniter was moved into place above the sample surface. This process can be seen in Fig. 2.10. Time to ignition was noted once the sample reached sustained burning and the test proceeded until the flame extinguished. The soot filter was than weighted again and compared to the original to figure out the soot production during the entire test. In order to make sure that the moisture produced during the combustion didn't affect the results, the filter was dried for a day in a convection oven at 75 C, before and after the test. This was done for several representative tests, but it had no effect on the final result. Therefore the rest of the tests were performed without the drying process.

Figure 2.1 FAA pressure modeling facility.

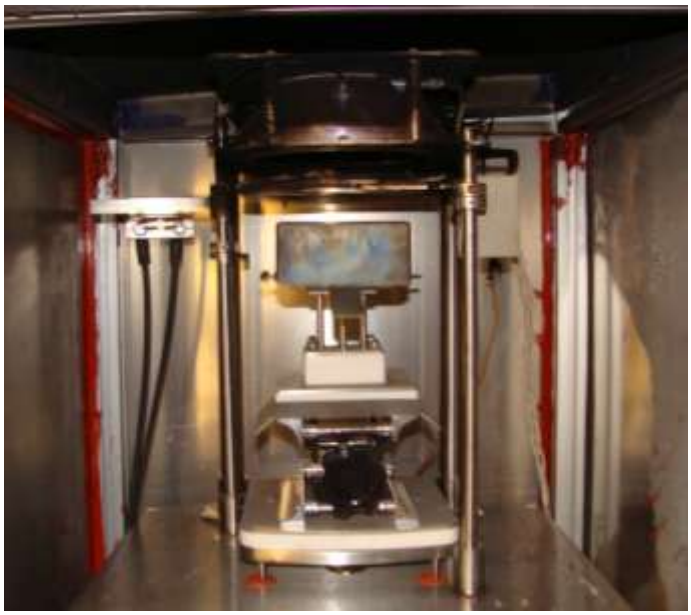

Figure 2.2 Standard mass loss calorimeter.

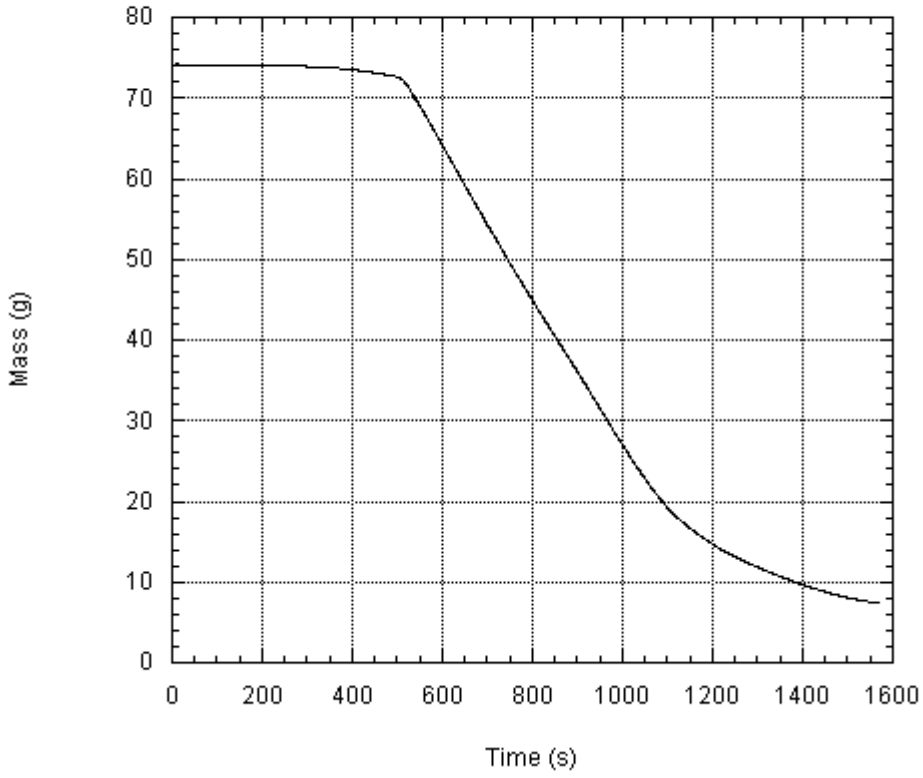

Figure 2.3 Mass loss for PMMA at 0.68 atm with 10 kW/m^2 external heat flux.

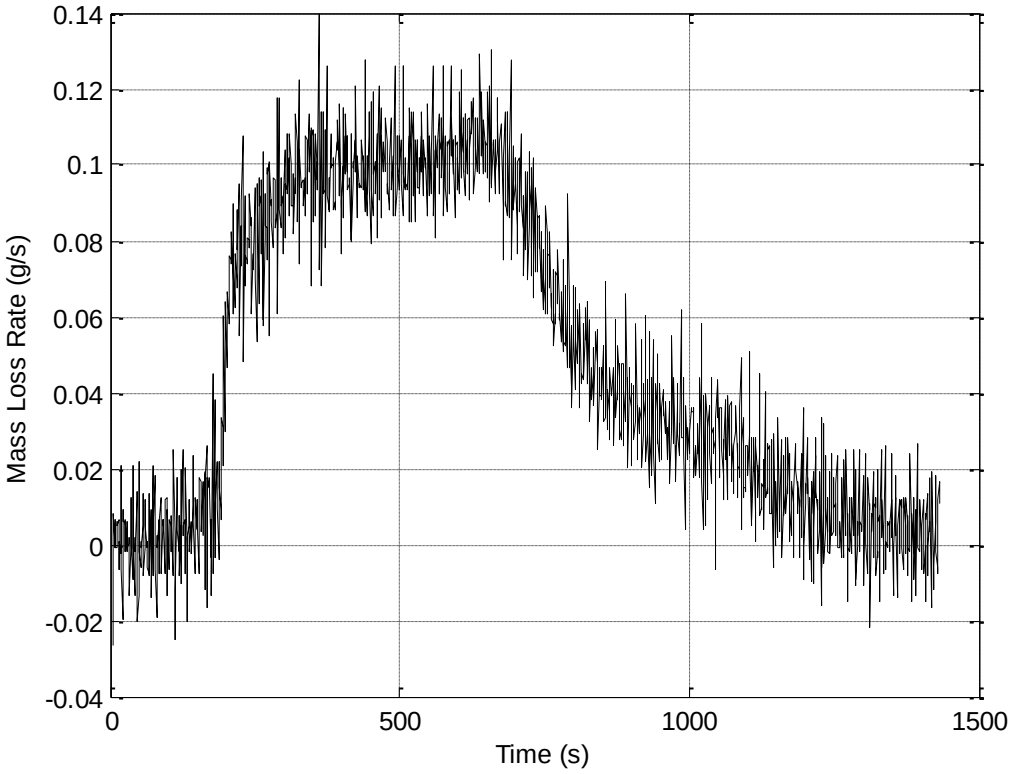

Figure 2.4 Mass loss rate for 0.68 atm with a 16 kW/m^2 external heat flux.

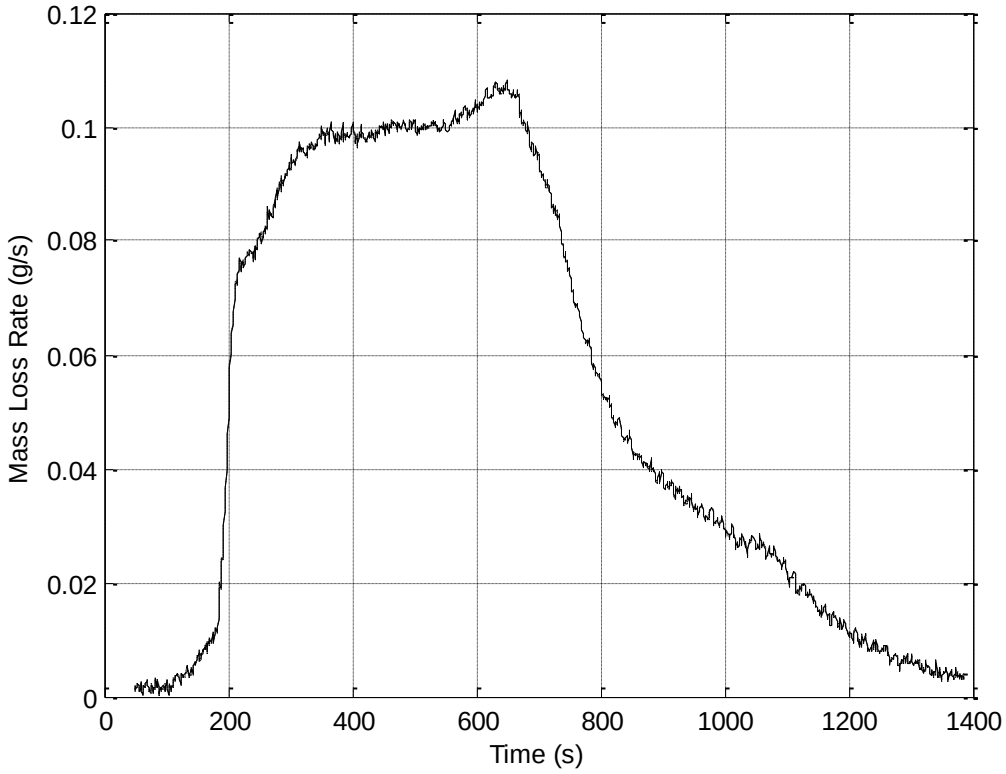

Figure 2.5 Mass loss rate for 0.68 atm at 16 kW/m^2 external heat flux, smoothed using a linear 21 point Savitzky-Golay filter.

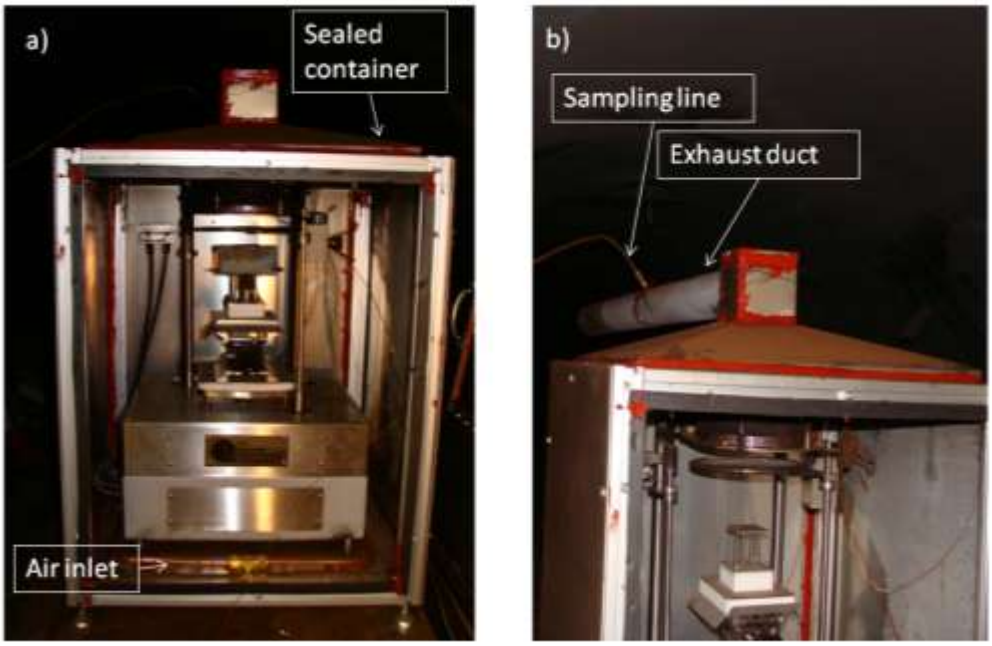

Figure 2.6 a) Front view. b) Side view. Enclosure holding the mass loss calorimeter, with an air supply fed through the bottom and exhausted out the top.

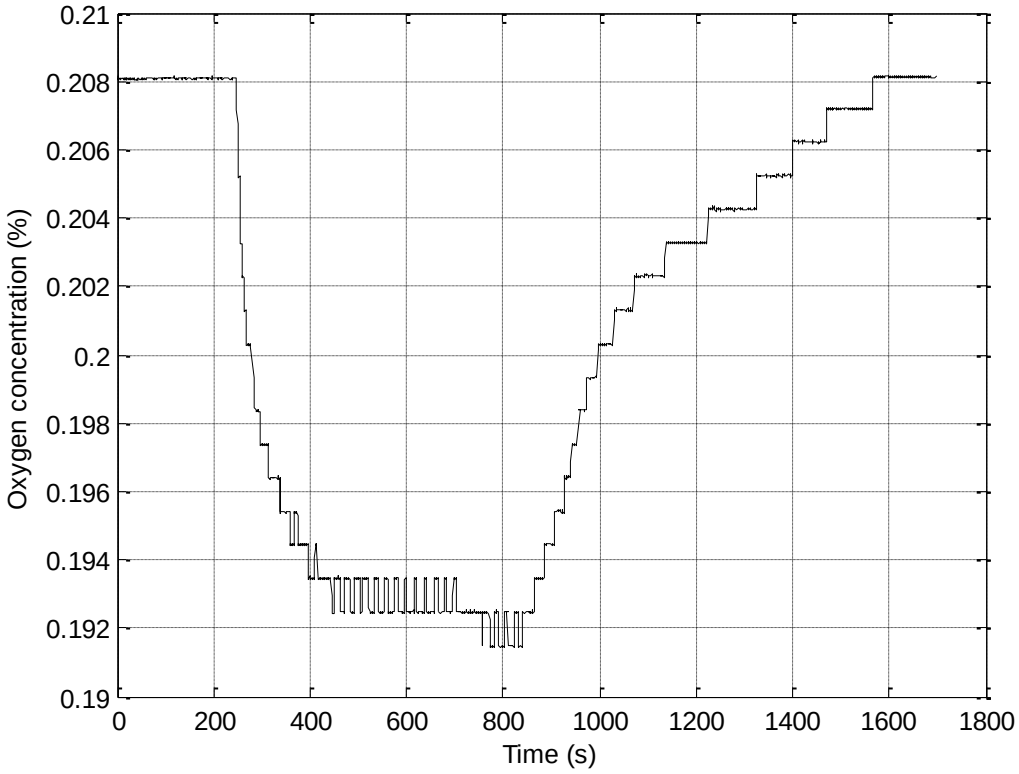

Figure 2.7 Oxygen consumption measurement at 0.68 atm with 16 kW/m^2 external heat flux.

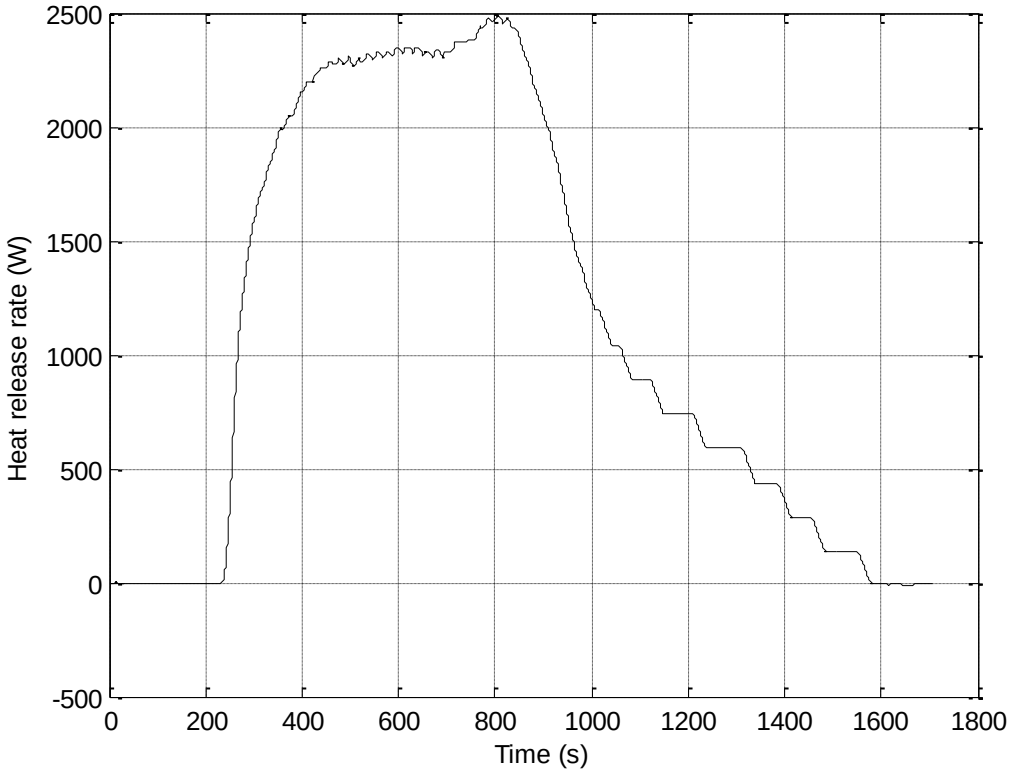

Figure 2.8 Heat release rate calculated from oxygen consumption.

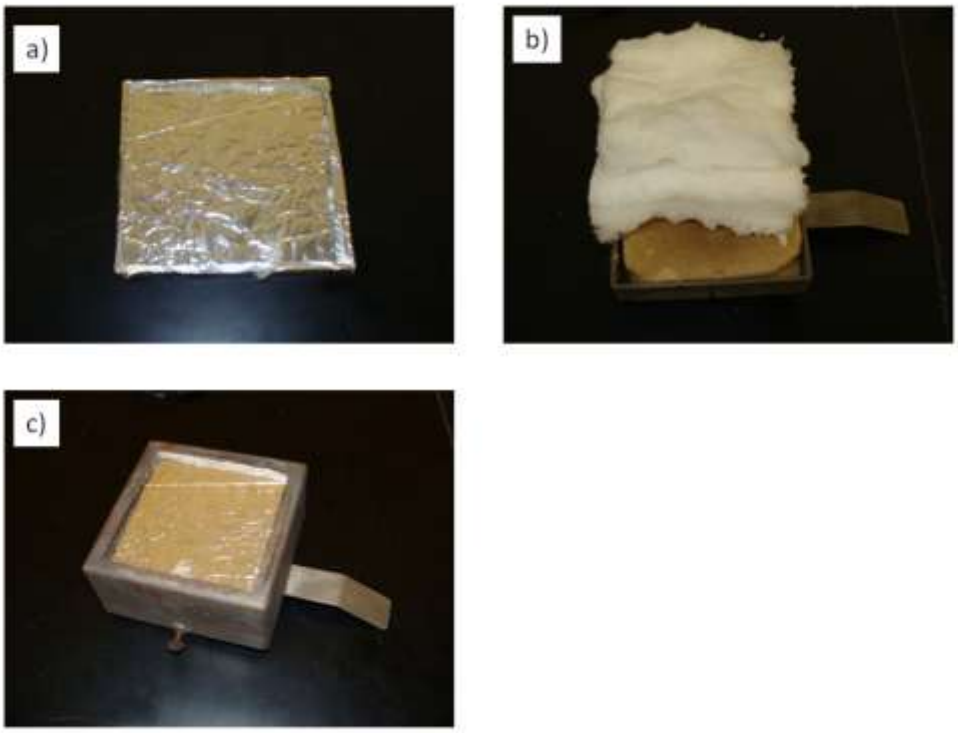

Figure 2.9 a) Sample is wrapped in an aluminum foil to prevent spillage. b) The insulation material is placed in the holder to reduce the heat transfer at the back surface. c) The sample is places in a steel holder.

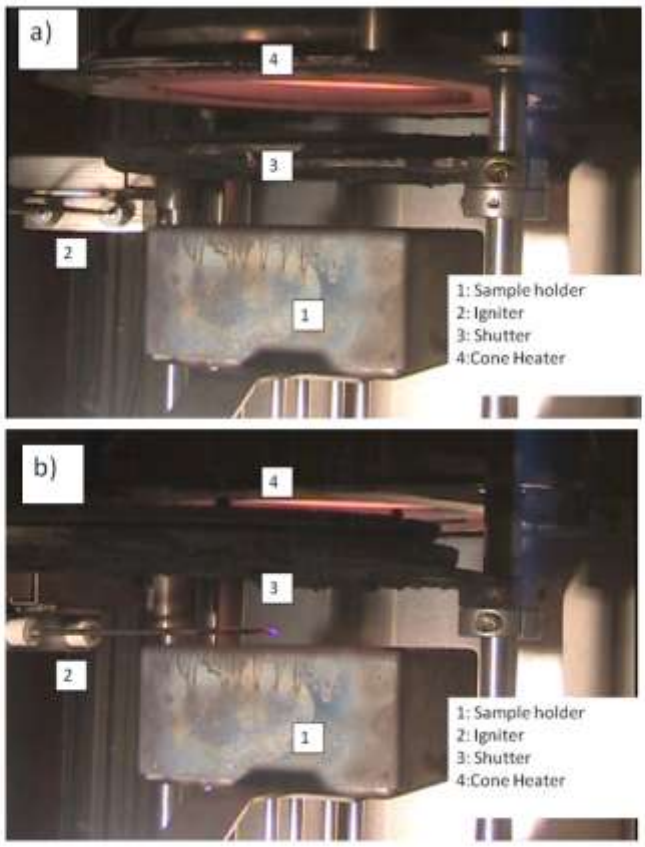

Figure 2.10 a) The system configuration before the test begins. b) The test begins. The shutter is opened and the igniter is moved above the sample.

Chapter 3

Theory

3.1 Ignition delay time

Ignition of a solid can be characterized by three distinct processes that together contribute to the total ignition time [18]. Initially the sample has to be brought up to the vaporization temperature generating combustible gases. The second step involved the transport and mixing of the fuel and the oxidizer. The last step is the time necessary for the mixture to go in to thermal runaway. Step 2 and 3, termed the mixing time and chemistry time, are usually orders of magnitude smaller compared with the pyrolysis time [18].

If the sample is of sufficient thickness, it can be approximated as a semi-infinite medium using the following equation:

$$\rho c \frac{dT}{dt} = k \frac{d^2T}{dx^2} \tag{3.1}$$

with boundary conditions for a constant heat flux at the surface:

$$-k \frac{dT}{dx} = \dot{q}'' \tag{3.1a}$$

$$T = T_\infty \qquad x \to \infty \tag{3.1b}$$

and initial condition:

$$T = T_\infty \quad t = 0 \tag{3.1c}$$

The solution can be found in most heat transfer textbooks as [19]:

$$T(x,t) - T_\infty = \dot{q}" \left[\frac{2\sqrt{t}}{\sqrt{\pi}\sqrt{k\rho c}} e^{(-\frac{x^2}{4\alpha t})} - \frac{x}{k}(1 - erf\, \frac{x}{2\sqrt{\alpha t}}) \right] \quad (3.2)$$

where x is the distance below the surface and $\alpha = k/c\rho$ is the thermal diffusivity. T_∞ is the ambient temperature, k is the thermal conductivity, c is the specific heat and ρ is the density. At time t_{ig} the temperature at x=0 becomes the ignition temperature T_{ig}. Eq. 3.2 now simplifies to:

$$T_{ig} - T_\infty = \frac{2q"\sqrt{t_{ig}}}{\sqrt{\pi}\sqrt{k\rho c}} \quad (3.3)$$

Eq. 3.3 can be rearranged in the following manner:

$$\frac{1}{\sqrt{t_{ig}}} = \frac{\dot{q}"}{TRP} \quad (3.4)$$

where:

$$TRP = \left(\frac{\pi}{4} k\rho c\right)^{\frac{1}{2}} \left(T_{ig} - T_\infty\right) \quad (3.5)$$

TRP is called the thermal release parameter, and is very useful in assessing the resistance of a material to fire propagation. $\dot{q}"$ is the net heat flux to the surface and is defined as:

$$\dot{q}" = \dot{q}"_e - \sigma(T_{ig}^4 - T_\infty^4) - h_c \left(\left(T_{ig} - T_\infty\right) + \frac{\dot{q}"_{py}}{h_c} \right) \quad (3.6)$$

Where the $\dot{q}"_e$ is the external heat flux, σ is the Boltzmann constant $\dot{q}"_{py}$ heat loss due to pyrolysis gases being given off, h_c is the convective heat transfer

coefficient (James G. Quintiere suggested adding $\dot{q}"_{py}$ to Eq. 3.6, personal communication). The last two terms in Eq. 3.6 are termed critical heat flux (CHF), which is the minimum flux that will allow for the fire to initiate [20]. CHF is dependent on the test method and needs to be determined experimentally.

There are several unknowns in Eq. 3.6 that need to be addressed. T_{ig} and h_c are obtained from experimental data. $\dot{q}"_{py}$ can be found from a physical understanding of what happens at the onset of flaming combustion, which is analogues to what happens at the lower flammability limit (LFL). Mass flux at ignition can be found from the following equation [18]:

$$\dot{m}"_g = h_m\left(Y_F(0) - Y_{F,\infty}\right) \tag{3.7}$$

where h_m is the mass transfer coefficient defined as the convective heat transfer coefficient divided by the specific heat of the gas at constant pressure, $Y_F(0)$ the concentration at the surface and $Y_{F,\infty}$ is the ambient concentration. At the onset of ignition the values are $Y_{F,\infty}$ = 0 and $Y_F(0) = Y_{F,LFL}$. By knowing the heat of decomposition (Δh_{py}) of the material, the heat loss due to vaporization can be approximated with the following equation:

$$\dot{q}"_{py} = \left(\frac{\Delta h_{py}}{\Delta h_C}\right) Y_{F,LFL}\Delta h_{py} \tag{3.8}$$

Mass fraction of fuel ($Y_{F,LFL}$) at LFL can be approximated by assuming that all the chemical energy released is equal to the sensible energy used to raise the temperature of the products of combustion [18]. The assumption results in the following equation:

$$Y_{F,LFL}\Delta h_C = c_P\left(T_{F,crit} - T_\infty\right) \tag{3.9}$$

where Δh_C is the heat of combustion. $T_{F,crit}$ is the adiabatic flame temperature at the LFL [18]. Combining Eqs. 3.8 and 3.9, the last term in Eq. 3.6 can be approximated by the following:

$$\frac{\dot{q}"_{py}}{h_c} = \left(T_{F,crit} - T_\infty\right)\left(\frac{\Delta h_{py}}{\Delta h_C}\right) \tag{3.10}$$

3.2 Critical mass flux

Another important parameter in understanding combustion of solids is the critical mass flux at ignition. It can be found using the mass transfer theory for Pr and Sc =1, which is valid for air. Similarly to Eq. 3.8, the mass flux at ignition can be found by substituting $Y_{F,\infty}$ = 0 and $Y_F(0) = Y_{F,LFL}$ into Eq. 3.7. Therefore mass flux at ignition is:

$$\dot{m}" = (\frac{h_C}{c_P})Y_{F,LFL} \tag{3.11}$$

It has been shown that mass fraction at the lower flammability limit can be estimated using a critical (LFL) flame temperature. This assumption reduces to Eq. 3.11. Eq. 3.11 can be used to find the limiting oxygen mass fraction ($Y_{O_2,Lim}$) by replacing it with the fuel mass fraction and replacing the heat of combustion with the heat of combustion per unit mass of oxygen (Δh_{O_2}).

3.3 Burning rate

Performing a simple energy balance on the surface of a burning sample results in the following equation:

$$\dot{m}'' L = \dot{q}''_{ext} + \dot{q}''_{flame} - \varepsilon\sigma T_v^4 \tag{3.12}$$

where $\dot{m}$ is the mass loss rate, L is the heat of gasification accounting for the sensible heat and the heat of vaporization, $\dot{q}''_{ext}$ is the external heat provided by the cone heater, $\dot{q}''_{flame}$ is the flame heat flux, including the convective and radiative terms. The last term in Eq. 3.12 accounts for radiative losses, where ε is the emissivity, σ is the Boltzmann constant and T_v is the surface (vaporization) temperature of the sample. Rearranging Eq. 3.12 in the format of "y=mx+b" allows for the extraction of flame heat flux and the heat of gasification.

$$\dot{m}'' = (\frac{1}{L})\dot{q}''_{ext} + \frac{(\dot{q}''_{flame} - \varepsilon\sigma T_v^4)}{L} \tag{3.13}$$

Eq. 3.13 shows that by taking the slope of the mass flux versus the external applied heat flux you can extract the heat of gasification. The flame heat flux can be extracted from equating the last term of Eq. 3.13 to the y-intercept.

For steady, 1D burning with purely convective heating the mass loss rate can be derived from gas phase combustion, resulting in [18]:

$$\dot{m}'' = \frac{h}{c_p}\ln(1+B) \tag{3.14}$$

where h is the convective heat transfer coefficient, c_p is specific heat of the gas and B is the Spalding Transfer Number given by

$$B = \frac{Y_{O_2,\infty}(\Delta h_c / r) - c_p(T_v - T_\infty)}{L} \tag{3.15}$$

In Eq. 3.15 $Y_{o_2,\infty}$ is the oxygen mass fraction, Δh_c is the heat of combustion, r is the stoichiometric oxygen to fuel mass ratio, T_∞ is the ambient temperature and L is the heat of gasification. Quintiere suggests that Eq. 3.14 can be expressed similarly to Eq. 3.12 assuming that the radiative losses, the radiative component of the flame heat flux and the external heat-flux are known a priori [18]. The results are expressed in Eq. 3.16 [18].

$$\dot{m}''L = \frac{h_c}{c_p}\left(\frac{\lambda}{e^{\lambda}-1}\right)\left(\frac{Y_{o_2,\infty}\Delta h_c}{r}(1-X_r) - c_p(T_v - T_\infty)\right) + \dot{q}''_{f,r} + \dot{q}''_e - \sigma(T_v^4 - T_\infty^4) \quad (3.16)$$

λ is defined as where $\lambda = c_p\dot{m}''/h_c$, and X_r is the radiative fraction. Comparing Eq. 3.16 to Eq. 3.12 it can be shown that the flame heat flux $\dot{q}''_{flame}$ is composed of the radiative ($\dot{q}''_{f,r}$) and convective ($\dot{q}_{f,c}''$) components, where the convective component is defined as:

$$\dot{q}_{f,c}'' = \frac{h_c}{c_p}\left(\frac{\lambda}{e^{\lambda}-1}\right)\left(\frac{Y_{o_2,\infty}\Delta h_c}{r}(1-X_r) - c_p(T_v - T_\infty)\right) \quad (3.16a)$$

On the left hand side of Eq. 3.16 shows the energy needed for vaporization at steady state burning, while the right side shows the amount of heat flux being absorbed. Since both sides of the equation have the mass loss term, an iterative solution is needed. Taking a closer look at $(\lambda/e^{\lambda}-1)$ it can be shown that as the mass flux away from the surface increases it causes the convective heat transfer coefficient to decrease. This term called the blocking factor acts to increase the boundary layer due to blowing caused by fuel vaporization. Since the induced

flow caused by the vaporization is in the opposite direction to the heat transfer it decreases the amount of energy being transfer back to the surface.

Flame emissivity is approximated as [21]:

$$\varepsilon = 1 - e^{\kappa L} \tag{3.17}$$

The κ is the effective soot emitter parameter, and L is the path length. Assuming a homogeneous gray mixture the path length can be approximated using a mean beam length ($L_{m,f}$) [21].

$$L_{m,f} = 4\frac{V}{A_S} \tag{3.18}$$

V is the volume of the flame and A_S is the surface area. Approximating the flame as a right cylinder emitting to its base, the mean beam length can be approximated with the following equation:

$$L_{m,f} = 0.65\left(\frac{\frac{l_f}{D}}{\frac{l_f}{D}+\frac{1}{2}}\right)D \tag{3.19}$$

where l_f is the flame length and D is the effective flame diameter, given as:

$$D = \frac{2}{\sqrt{\pi}}S \tag{3.19}$$

S is the length of one side of the square sample. The length of the flame is given using a Heskestad flame length model as [22]:

$$\frac{l_f}{D} = 0.23\ \frac{\dot{q}^{\frac{2}{5}}}{D} - 1.02 \tag{3.20}$$

where $\dot{q}$ is the heat release rate (HRR) in kW. $\dot{q}$ can be obtained from the mass loss rate as follows:

$$\dot{q} = \Delta h_C \cdot \dot{m} \tag{3.21}$$

In the previous equation Δh_C is the heat of combustion and $\dot{m}$ is the mass loss rate. The radiative flame heat flux scales can be expressed as follows:

$$\dot{q}''_{f,r} = \sigma(T^4_{Flame} - T^4_V)(1 - e^{\kappa L_{m,f}}) \tag{3.22}$$

where κ is the flame emissivity, $L_{m,f}$ is the mean beam path length, and T_{Flame} is the average flame temperature, defined as [18]:

$$T_{Flame} = T_\infty + \frac{0.5(\Delta h_C/r)}{c_P}(1 - X_r)Y_{O_2,\infty} \tag{3.22a}$$

3.4 Pressure Dependence

There are two places in the previous analysis where the pressure has any effect. The first one comes in through the convective heat transfer coefficient, and the second one comes in through the emissivity of the soot. The emissivity of the soot is proportional to the soot volume fraction.

For laminar natural convection the average convective heat transfer is a function of the Grashof number, Eqs. 3.23-26 [23]. The pressure effect comes in through the density change, Eq. 3.25, and therefore it can be shown that the effect of pressure on the average heat transfer coefficient and conversely the mass loss varies as $P^{1/2}$.

$$\bar{h} = \frac{\overline{Nu}_L k}{L} \tag{3.23}$$

$$\overline{Nu_L} = .15(\mathrm{Pr} Gr_L)^{1/4} \tag{3.24}$$

$$Gr_L = \frac{gL^3\rho^2}{\mu}(\frac{\Delta\rho}{\rho}) \tag{3.25}$$

$$h \propto P^{1/2} \tag{3.26}$$

The radiative component is also affected by the reduction in pressure. According to de Ris *et al.*(2000), the emissivity of the flame scales with pressure as P^2 [24]. Therefore the radiative flame heat flux scales with pressure as:

$$\dot{q}''_{f,r} = \sigma(T_{Flame}^4 - T_V^4)(1 - e^{\kappa L_{m,f}}) \tag{3.27}$$

Given that pressure and oxygen effects are now known a simpler relation can be formulated to show how mass loss is affected. The convective flux can be shown to be proportional to pressure and oxygen concentration:

$$\dot{q}''_{f,c} \propto P^{1/2} Y_{O_2,\infty} \tag{3.28}$$

For small values of K and $L_{m,f}$, it can be shown that $(1 - e^{\kappa L_{m,f}}) \propto P^2$ and from Eq. 3.22a, $T_{Flame} \propto {Y_{O_2,\infty}}^4$, therefore:

$$\dot{q}''_{f,r} \propto (P^{1/2} Y_{O_2,\infty})^4 \tag{3.29}$$

It can therefore be shown that if all other parameters are invariant with oxygen and pressure that the following relation should hold true:

$$m'' - \frac{\dot{q}''_{net}}{L} \propto (P^{1/2} Y_{O_2,\infty}) \tag{3.30}$$

Chapter 4

Results and Discussion

4.1 Mass Flux

Although there have been many studies of combustion of PMMA at ambient conditions, not much has been done in a high altitude environment. Given that the materials that are found in an airplane will encounter low pressure environments on a daily basis, the standard testing methods may not be adequate. In order to be able understand the effect of low pressure environment a mass loss calorimeter was setup in a vacuum chamber capable of simulating altitudes up to 48,000 feet.

In order to be able to compare samples of different sizes the results for mass loss rate were divided by the cross-sectional area. This also allows for the experimental results to be compared with theory. The Initial step was to extract the heat of gasification from the experimental data. A 10cm x 10cm square PMMA sample was exposed to several different external heat fluxes. Eq. 3.13 shows that if the mass flux is plotted against the external heat flux the slope of the line is the inverse of the effective heat of gasification. Following this logic the mass flux was plotted versus external heat flux in figure 4.1.

The measured effective heat of gasification is 3.58 +/- 2 kJ/g. Tewarson (2002) found the heat of gasification to be 1.6 kJ/g [20], while Rhodes found his to be 2.77 kJ/g [26]. The large error associated with the calculated heat of

gasification is due to the uncertainty in the steady mass flux for external heat fluxes at 50 and 75 kW/m^2.

4.2 Mass Flux at lower pressure and oxygen concentrations

The samples were burned at pressures ranging from ambient to 0.18 atm. The resulting steady mass flux rate was plotted against pressure for different external heat fluxes in Fig. 4.2 a-c. The plots show a reduction in fire intensity at all levels of external heat fluxes. The most significant difference occurs at the lowest pressure where there is a threefold reduction in steady state mass flux. At 25 kW there is only a 26 % reduction, indicating that for a larger fire the pressure effect is limited.

For external heat fluxes of 50 and 75 kW/m^2, the sample did not reach steady burning. This is mainly due the fact that the sample burned up before the time required for steady burning to occur. A thicker sample would need to be tested to get a more certain result. The results presented here are for the average burning rate. The results for those heat fluxes can be seen in Figs. 4.3 a-d, where the mass flux is plotted versus external heat flux. The error bars are reflecting the uncertainty of the measurement, since the sample didn't achieve steady burning. The average mass flux only showed a 15 % reduction between ambient and 0.18 atm.

Several tests were performed at different oxygen concentration ranging from 21 to 12 %, with external heat flux at 16 kW/m^2. The tests were repeated at different pressures and the results were plotted in Figs. 4.4 a-d. The plots show a

reduction in the mass flux at lower oxygen mass fractions, which is consistent with the fact that the flame temperature decreases at lower oxygen levels. The effect is diminished at the lowest pressure. There the heat flux form the flame is low enough that the temperature change associated with the oxygen level is not as relevant. It was also observed that the sample would not ignite below 16 % oxygen. This is in contrast to the samples at ambient pressure where the sample ignited at 12 % oxygen.

In chapter three a formulation was derived that showed a simple relation between external heat flux, pressure and oxygen concentration. The resulting equation was given by Eq. 3.25.

The formulation can be rearranged so that the left hand-side is only a function of the product of $P^{1/2}$ and $Y_{O_2,\infty}$. When the experimental data was plotted in this manner, all the data collapsed onto a single line. The results can be seen in Fig. 4.5.

The results for 50 and 75 kW were excluded as steady state mass loss was not reached. The plot in Fig. 4.5 shows a universal curve for all external heat fluxes, pressures and oxygen concentrations. The resulting curve was then fitted resulting in the following power law:

$$\dot{m}'' - \frac{\dot{q}''_{net}}{L} = 73.2\left(P^{1/2}Y_{O_2,\infty}\right)^{1.4} \tag{4.1}$$

It was shown in chapter 3 that the convective term scales as $P^{1/2}Y_{O_2,\infty}$, and the radiative term as $\left(P^{1/2}Y_{O_2,\infty}\right)^4$. This suggests that the convective heat transfer

plays a more dominant role in the process, but at the same time radiation cannot be ignored. This particular scaling might work well for PMMA, but it's unknown if the relation will hold for other polymers. Since the soot production will change, depending on the polymer, the resulting radiative component will change accordingly. It is also not clear whether the relation will hold above ambient conditions, since no tests were performed above ambient pressure or oxygen concentration.

4.3 Time to Ignition

Another important parameter that indicated material flammability is the time to ignition. This parameter can be considered a sum of three distinct steps that help contribute to the delay of ignition. Initially the solid has to be heated to a high enough temperature to cause pyrolysis gases to be given off [18]. The second step involves the transport of the fuel through the boundary layer and the mixing of the fuel with the oxidizer. The last time step involves the time it takes for the chemical to go into thermal runaway.

One way to plot the time ignition is versus the external heat flux. The results for ambient pressure are plotted in Fig. 4.6. The plot shows data that time to ignition raises exponentially with the reduction of the external heat flux. As shown before time to ignition can be calculated using the following equation:

$$\frac{1}{\sqrt{t_{ig}}} = \frac{\dot{q}''}{TRP} \tag{4.2}$$

If the data is plotted in this way it can be seen that the TRP is the inverse of the slope of the fitted line. The resulting plot can be seen in Fig. 4.7 giving TRP = 346 kW-s$^{1/2}$/m^2. Knowing TRP, the only unknowns left in Eq. 3.1 are the Tig and the effect of decomposition $\dot{q}"_{py}$.

The $\frac{\dot{q}"_{py}}{h_c}$ term can be calculated using Eq. 3.10. Δh_{py} and Δh_C were measured and found to be 0.87 kJ/g [27], and 24.2 kJ/g [20], respectively. Similarly $T_{F,crit}$ is obtained experimentally and found to be 1300 °C [18]. The critical heat flux can now be found from the following equation:

$$\dot{q}"_{cr} = \sigma\left(T_{ig}^4 - T_\infty^4\right) + h_c\left(\left(T_{ig} - T_\infty\right) + 48.5°C\right) \tag{4.3}$$

Taking T_{ig} to be 275 °C [29], $\dot{q}"_{cr}$ is found to be 8.25 kW/m^2. Plugging Eq. 3.3 back into 3.1 it can be seen that the theory doesn't represent the data very well. The major flaw of the model is its inability to account for the change in slope near the critical heat flux. Data in Fig. 4.6 suggests that the critical heat flux is around 10 kW/m^2, while Fig. 4.7 implies that the critical heat flux is less than 0. The theory, on the other hand, describes a line with a slope of 1/TRP and x-intercept at 8.25 kW/m^2.

The theory in Eq. 3.6 is therefore adjusted by a constant (James G. Quintiere, personal communication) giving:

$$\dot{q}" = \dot{q}"_e + C - \sigma(T_{ig}^4 - T_\infty^4) - h_c\left(\left(T_{ig} - T_\infty\right) - \frac{\dot{q}"_{py}}{h_c}\right) \tag{4.4}$$

where C is 15.8 kW/m^2. The experimental results versus the corrected theory are plotted in Fig. 4.8. In order to measure the repeatability, the tests were repeated 6-7 times for pressure of 0.18, 0.47 and 1 atm at 16 kW/m^2. The resulting spread was +/- 30 s, and was used to plot the error bars for the rest of the data.

Ignition delay times were measured alongside the mass loss rate. Time to ignition was plotted versus pressure in Fig. 4.9 for several external heat fluxes. Similarly to mass loss rate the effect of pressure on ignition delay time is diminished at higher external heat flux. The strongest effect can be seen for heat flux of 10 kW, where the ignition time decreases by 30% from 1 to 0.18 atm. Since the majority of fire tests are performed at ambient conditions, the effect of pressure is usually not considered. But as shown above pressure does play a role in material flammability and must therefore be taken into account.

The equation for time to ignition derived in chapter 3 can be combined with the analysis of the heat transfer coefficient to try to develop a theory for the time to ignition at various pressures. As such Eq. 3.4 can be modified to account for the change in pressure as follows:

$$\dot{q}" = \dot{q}"_e + C - \sigma(T_{ig}^4 - T_\infty^4) - h_c(P)^{1/2}\left(\left(T_{ig} - T_\infty\right) - \frac{\dot{q}"_{py}}{h_c}\right) \qquad (4.5)$$

where P is the total pressure and P_∞ is the ambient pressure (14.7 psia). Eq. 3.5, when substituted back into Eq. 3.1, can now be used to solve for the time to ignition at different pressures. The comparison between the calculated and measured ignition times can be seen in Fig. 4.9.

The model shows good a good agreement with the results at higher external heat fluxes but fails below 16 kW/m^2. The theory does predict a reduction of the ignition delay time with a decrease in pressure, and that it trends with the one-half power with the pressure. Looking back at Fig. 4.7 it can be observed that close to the critical heat flux the experimental results suggest that the plot should curve down and intersect the x-axis at the critical heat flux of 8.25. This doesn't happen with the theory, where a $\frac{1}{\sqrt{t_{ig}}}$ scaling is obtained. So although the theory works well for higher heat fluxes, the conditions close to the critical heat flux are not very well represented by this theory.

4.4 Mass flux at ignition

Piloted ignition of solids can be characterized by two phenomena, flashpoint and fire-point. Flashpoint is characterized by the conditions under which the pyrolysis products achieve the LFL , while fire-point corresponds to the condition where the flame can sustain itself. The fire-point is dependent on whether the heat flux from the flame is sufficient in raising the surface temperature, where enough pyrolysis gases are produced to sustain flaming combustion. In an open system these terms can be characterized by their mass fluxes, which can be measured. The empirical results for the fire-point suggest that it is the 1.87 times larger than the flashpoint [29].

Taking a closer look at Fig. 2.5, there is a subtle increase in mass flux before the sample ignites. There is a critical value for the fuel mass flux in order for the sample to reach ignition. McAllister *et al.* (2010) suggest that since the oxygen

mass flux changes with pressure, and LFL doesn't, then the critical fuel mass flux at ignition would also change [12]. As the pressure goes down, density of air is lower, thereby reducing the amount of available oxygen per unit volume. This in turn lowers the amount of fuel needed to reach the lower flammability limit. Similar observations were observed by Fereres *et al.* (2011) in a horizontal, forced convection apparatus [30].

Since the ignition process takes several steps, there is a slight delay between the time the critical heat flux is achieved and the actual ignition. It can be seen in Fig. 2.5 that the mass flux is more or less constant for some duration before the sample ignites. An average of 20 points was therefore taken to calculate the mass loss rate at ignition. The results were plotted along-side Eq. 3.11, derived in chapter 3.

The resulting mass fluxes were compared to the theoretical results in Fig.4.11, showing good agreement. The plots show a slight decrease of the mass flux at lower pressures, which is consistent with the theory. It is another indicator that in a low pressure environment the material is more flammable.

4.5 Effective heat of combustion

Another important property of the system is that if mass loss and oxygen consumption can be measured at the same time, it can be used to measure the effective heat of combustion. Walters et al. (1997) measured the heat of combustion for many different polymers and showed a very good agreement with tabulated values obtained with bomb calorimeter [31]. The heat of combustion is

a material property and hence shouldn't change with pressure. This is not necessarily a useless measurement as the efficiency of the combustion might change at different pressures. Since the HRR measurements using oxygen consumption assumes certain combustion efficiency, and any change would be reflected in the calculated heat of combustion.

An average of all the points between the peak value and 80 % of the peak value were taken for both mass flux and heat release rate. The resulting mean values were used to calculate the effective heat of combustion. The region of interest used to calculate the average can be seen in Fig. 4.12.

A Matlab program was written to calculate the averages and then calculated the effective heat of combustion using,

$$\Delta h_C = \frac{\dot{m}}{HRR} \tag{4.6}$$

where $\dot{m}$ is the average mass loss rate, and HRR is the heat release rate calculated using oxygen consumption calorimetry. The oxygen consumption measurement was taken for all the tests, and the resulting averages for different pressures were plotted in Fig. 4.13. The averages consist of ambient oxygen concentration as well as those at lower oxygen concentrations. The error bars show the scatter in the data. The actual heat of combustion, calculated using a bomb calorimeter is 24.2 kJ/g [20]. The error bars are +/- 5% [17], which is the accuracy of the method used. The data is overestimating the actual heat of combustion, but the relative change from tests at different pressures is mostly

unchanged. The heat of combustion should remain constant at different pressures, since it's a material property. Therefore if there is any variation in the calculated heat of combustion at different pressure it would indicate that the combustion efficiency changed. This would be consistent with some visual observations that the flame became less sooty.

4.6 Soot Yields

Soot plays a very important part in the radiative heat transfer of the flame in a fire. A flame that is sootier is able to transfer more of its energy back to the sample surface, and increase the burning rate. A sample line was inserted in the exhaust stream of the setup, and a paper filter was used to collect the soot particles. The weighted soot accumulation was scaled with the total mass loss during the tests and the results are plotted in Fig. 4.15. The error bars are associated with the scatter of 2-3 repeated tests at 16 kW/m^2, for .18, .47 and 1 atm. The rest of the results are single tests, but since the scatter didn't change much going from 1 to .18 atm, it was assumed that the scatter is about constant.

All the tests show a similar trend of reduced soot production at lower pressures. This results shows that the radiative term can't be treated as a constant and has to take pressure variations into account.

It could be argued that the soot concentration in the exhaust stream is proportional with the soot volume fraction in the flame. Fitting the results for the soot yield vs pressure gives a power law relation between $P^{0.7}$ and $P^{1.22}$. This is

in contrast to P^2, which was argued using dimensional analysis by de Ris [24]. His results might still be valid for larger fires where the flames are turbulent.

4.7 Flame characterisics

4.7.1 Flame Color and shape

The color and the shape of the flame can provide some insight into how the flame is transferring energy back ot the sample. A color change from a bright yellow to a dim blue color might indicate a redction in soot production, hence reducing the radiative heat transfer to the sample surface. It was shown in chapter 3 that the convective heat transfer is proportional to $P^{1/2}$. Pressure is linearly proportianl with density throught the ideal gas law, therefore a reduciton in pressure will also correspond to the reduction in denisty. Since denisty variation is the driving force for the convective heat transfer, a reduction in density causes a net decrease in the amount of energy transferred back to the sample.

Visual observation of the flames during the tests showed a substantial change in flame color, going from ambient to low pressure environments. The flame changed from being luminous and yellow to, a dim blue color. The flame shape and profiles can be seen in Fig. 4.16.

The buoyancy effect is difficult to see in flame with no external heat flux. Since the mass flux is so small at low pressure, the flame can only be sustained close to the surface. When the sample was exposed to external heat flux of 50 kW/m^2, the buoyancy effect becomes more noticeable, as seen in Figs. 4.17. The

flame with no external heat flux transitions from turbulent to a laminar regime, at lower pressure. This is not as clear for the flame with an imposed external heat flux.

4.7.2 Flame Temperature

Since a temperature gradient is needed for heat transfer to proceed, any change in flame temperature will affect the burning behavior of the sample. Since the flame produces less soot at lower pressure, it will cause the flame to have lower radiative losses. This in turn should cause the equilibrium flame temperature to be higher. Due to the highly fluctuating nature of the flow, the best spot to measure the representative flame temperature was downstream inside the fully developed plume. Even then the fluctuations range around +/- 100 C.

Flame temperature measurements were taken using a K-type thermocouple. The thermocouple was placed 20 cm above the center of the sample for the duration of the test. The error bars in Fig. 4.17 with represent the temperature fluctuation, associated with the movement of the flame front across the thermocouple. The analytical expression for an average flame temperature in chapter 4, gives a value of 1050 C. This is within the margin of error for the measurements taken. According to the above results the average flame temperature stays relatively constant at different pressures.

4.8 Analytical Model

The simple analytical model, described in chapter 3, was implemented and compared to the data. The full explanation of the model is found in chapter 3.

The model needs several physical parameters that need to be inserted into the model for it to work. The convective heat transfer coefficient is taken to be 10 W/m^2-K [32]. de Ris (2000) measured K to be 1.3, and radiative fraction to be 0.34 [24]. The vaporization temperature was found experimentally to be 350-400 C [33]. The temperature used in the model was taken at 375 C. The only parameter that was modified was the heat of gasification. The only term that was not obtained experimentally was the heat of gasification. The value used was the one that gave the best fit, resulting in a value of 2.2 kJ/g.

Given that soot measurements were taken during some of the tests at different pressure, an attempt was made to use that trend in the model to simulate the variation of emissivity with pressure. The data suggests that soot varies linearly with pressure. The model was modified to incorporate this new scaling, and the results are as follows.

The model was solved and plotted in Matlab. The model uses a $P^{1/2}$ scaling for the convective heat transfer and P scaling for the soot emissivity. The results are compared with the experimental data in Fig. 4.2 for different external heat fluxes. The model seems to track the data, but at the higher heat fluxes it overshoots the results. The main reason is that the heat of gasification was a lot smaller compared to the experimental results. The particular heat of gasification was chosen because it gave the closest fit of the data, and falls between the results from Tewarson (1976) and Rhodes (1996). Given that the points at higher heat flux exposures didn't reach steady state burning, the uncertainty in those results is quite high. Further test at those heat fluxes need to be done to further

validate the model. The theory was then plotted versus pressure, Fig. 4.3, and oxygen mass fraction in Fig. 4.4. In both cases the theory is shown to be in very good agreement with the experimental results.

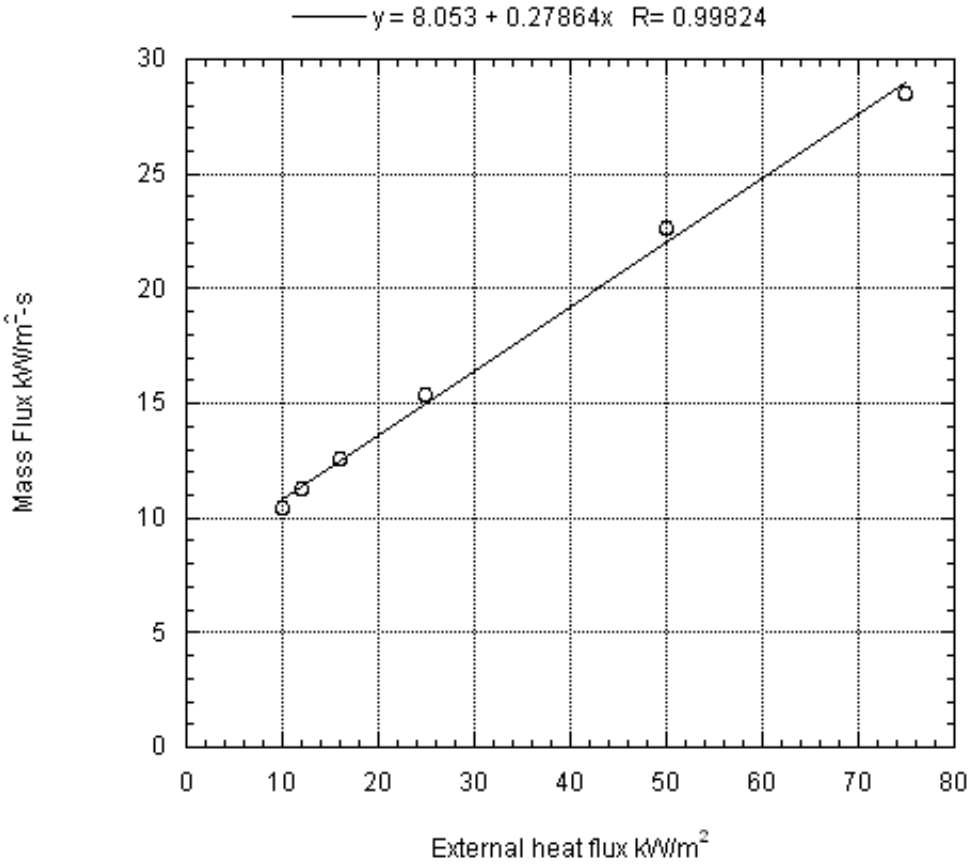

Figure 4.1 Experimental data fitted with a straight line, where the slope is the inverse of the heat of gasification.

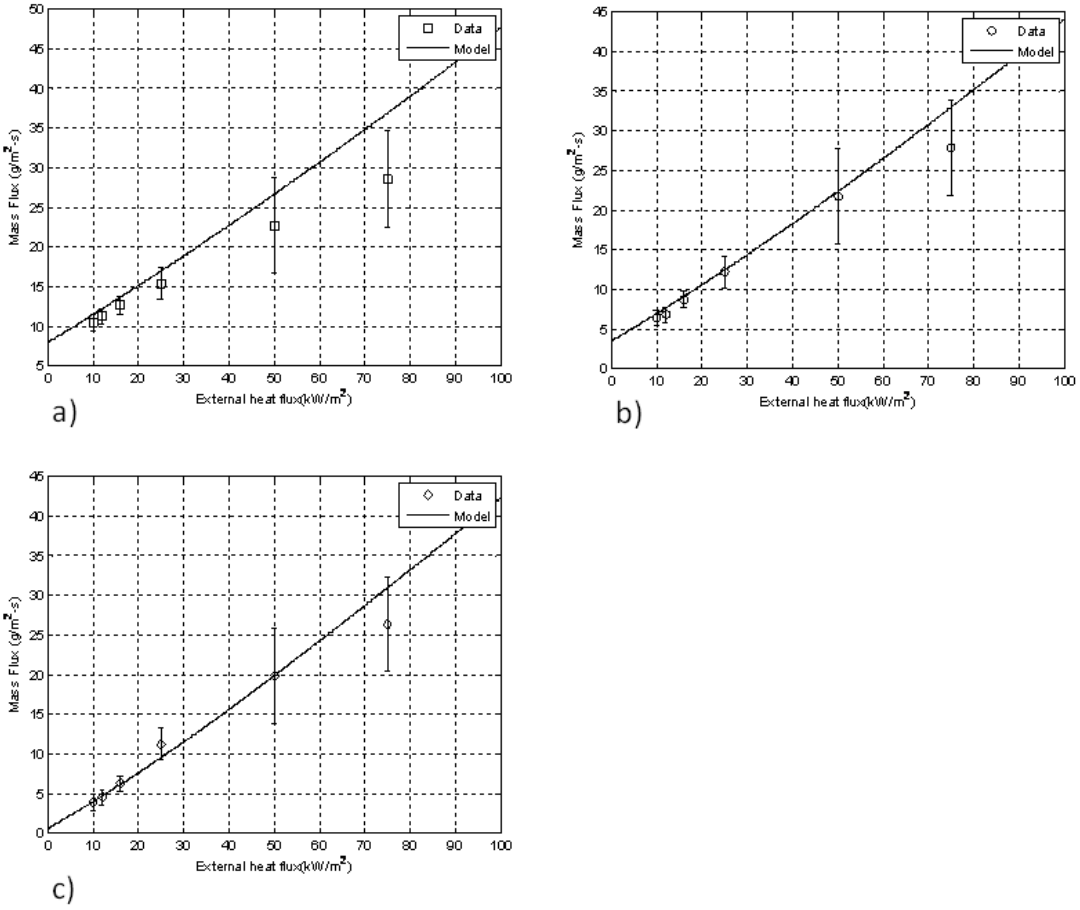

Figure 4.2 Mass flux versus heat flux at, a) 1 atm, b) .47 atm and c) 0.18 atm.

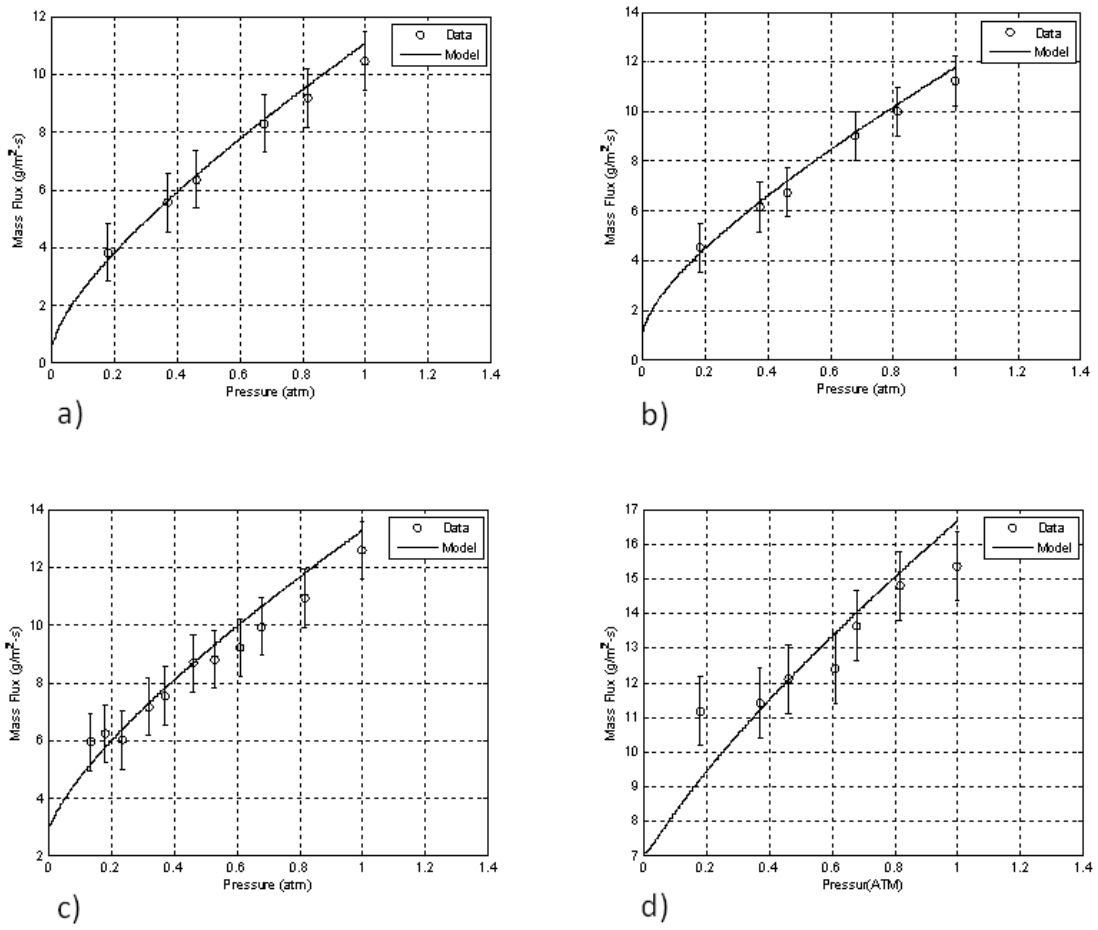

Figure 4.3 Mass flux versus pressure at a) 10 kW/m^2, b) 12 kW/m^2, c) 16 kW/m^2 and d) 25 kW/m^2.

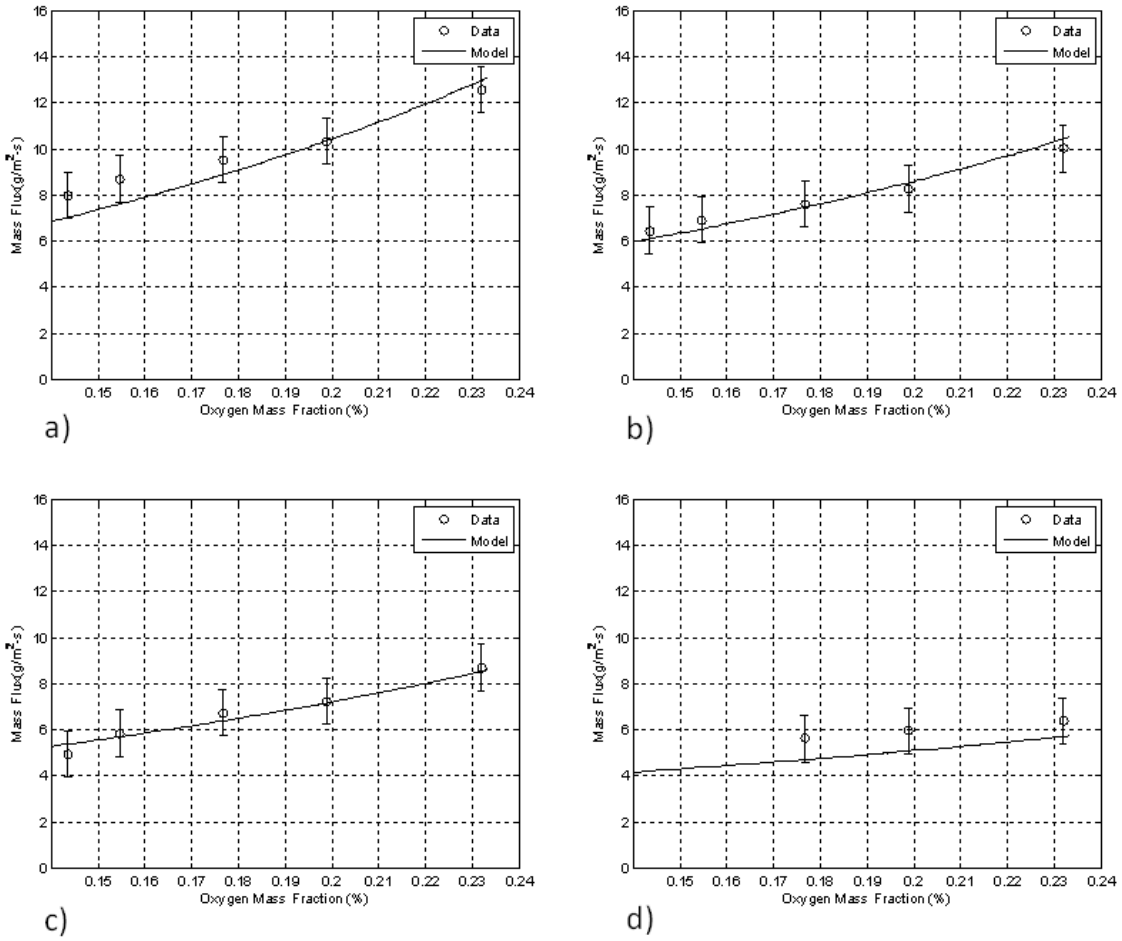

Figure 4.4 Mass flux versus oxygen mass fraction at a) 1 atm, b) 0.68 atm, c) 0.47 atm and d) 0.18 atm.

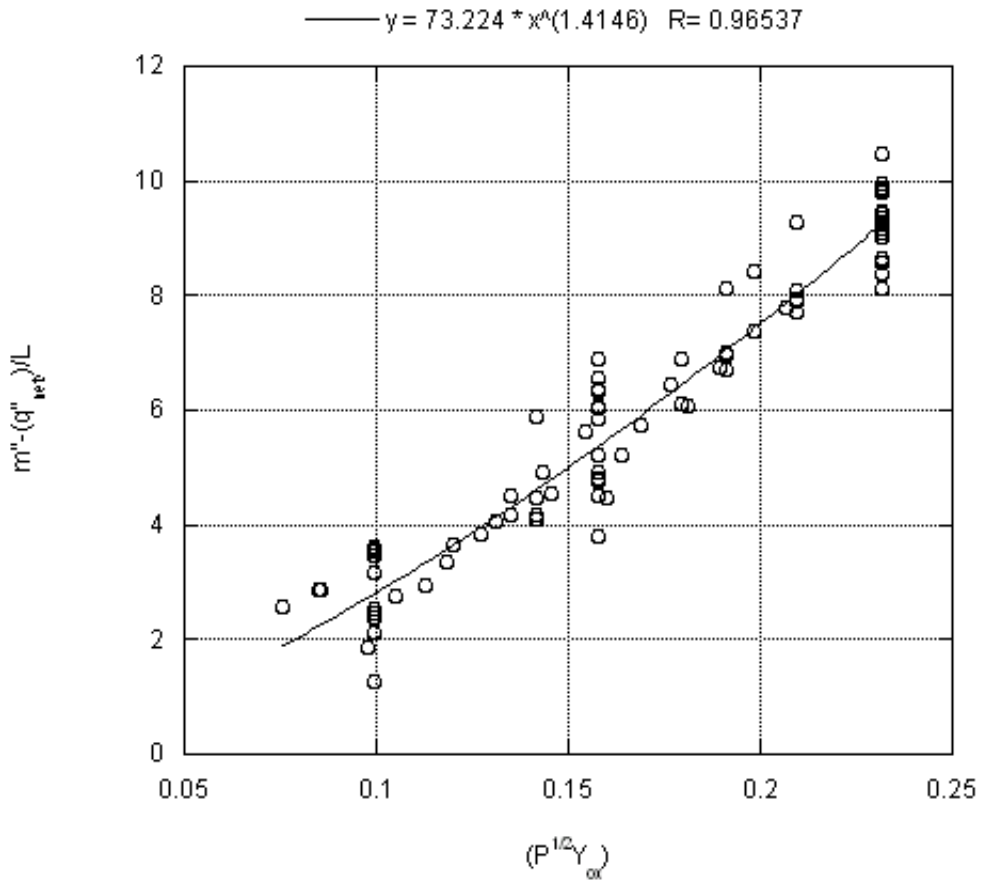

Figure 4.5 The experimental results plotted versus the product of pressure and oxygen concentration.

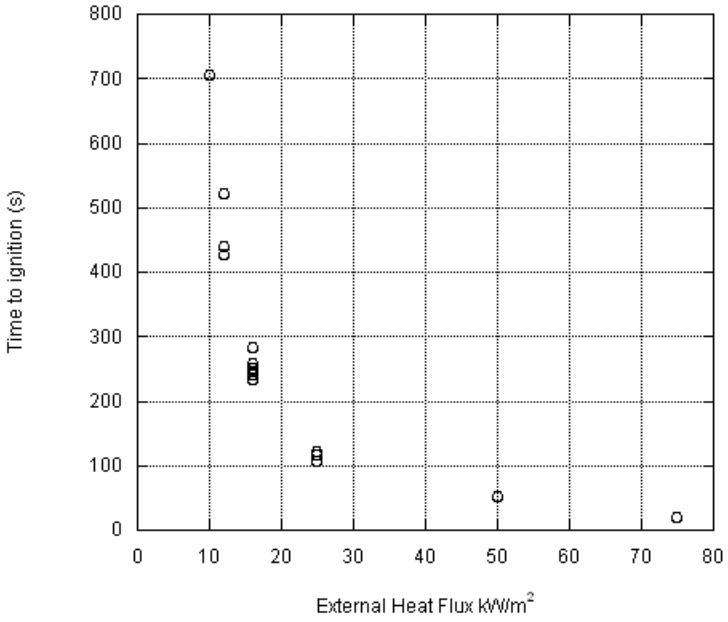

Figure 4.6 Time to ignition versus external heat flux shows a asymptotic behavior close to the critical heat flux.

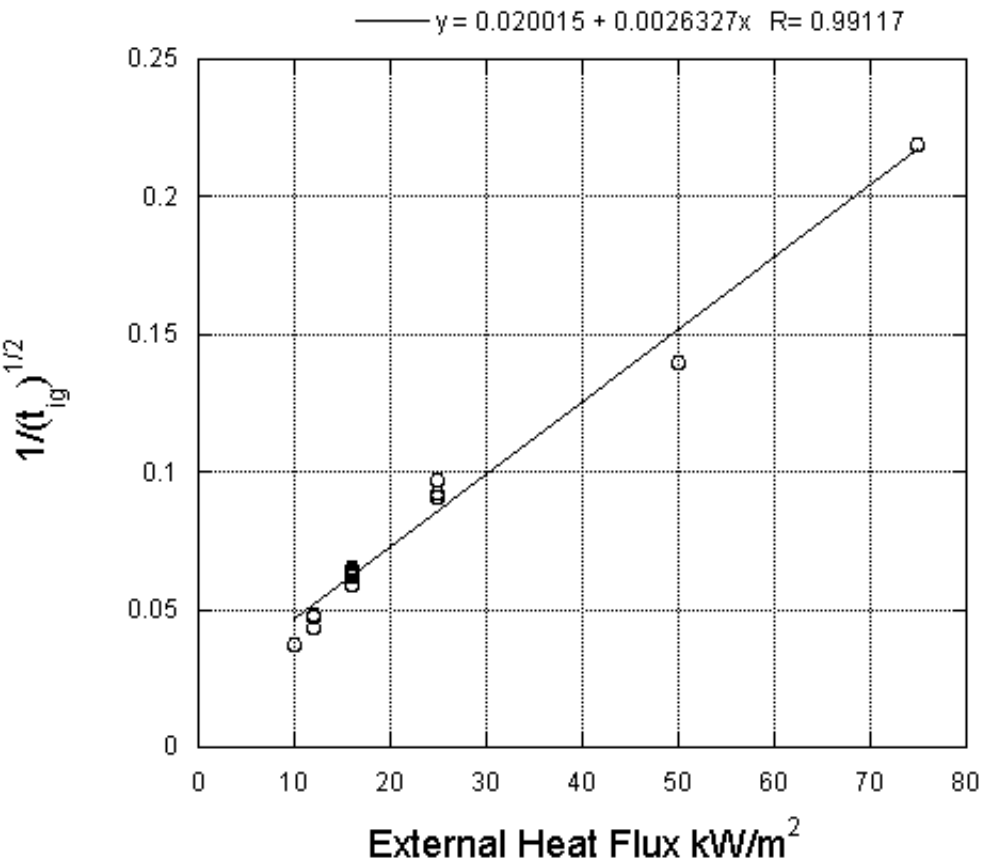

Figure 4.7 Ignition data for ambient condition fitted with a line.

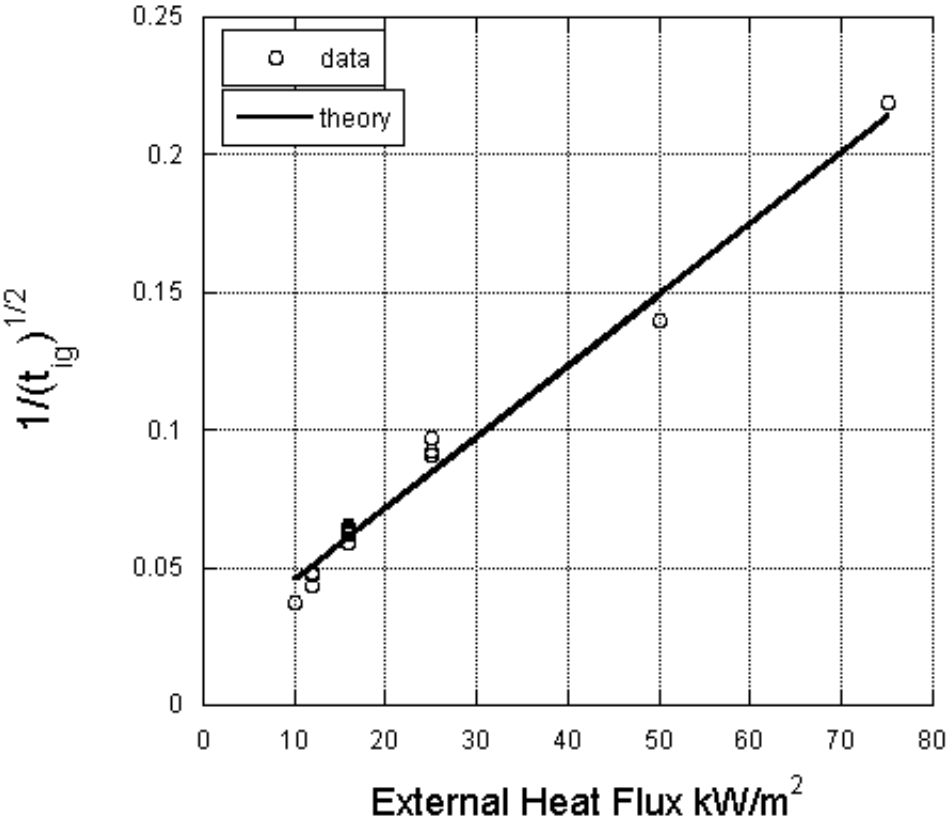

Figure 4.8 Theoretical model corrected to fit the experimental results.

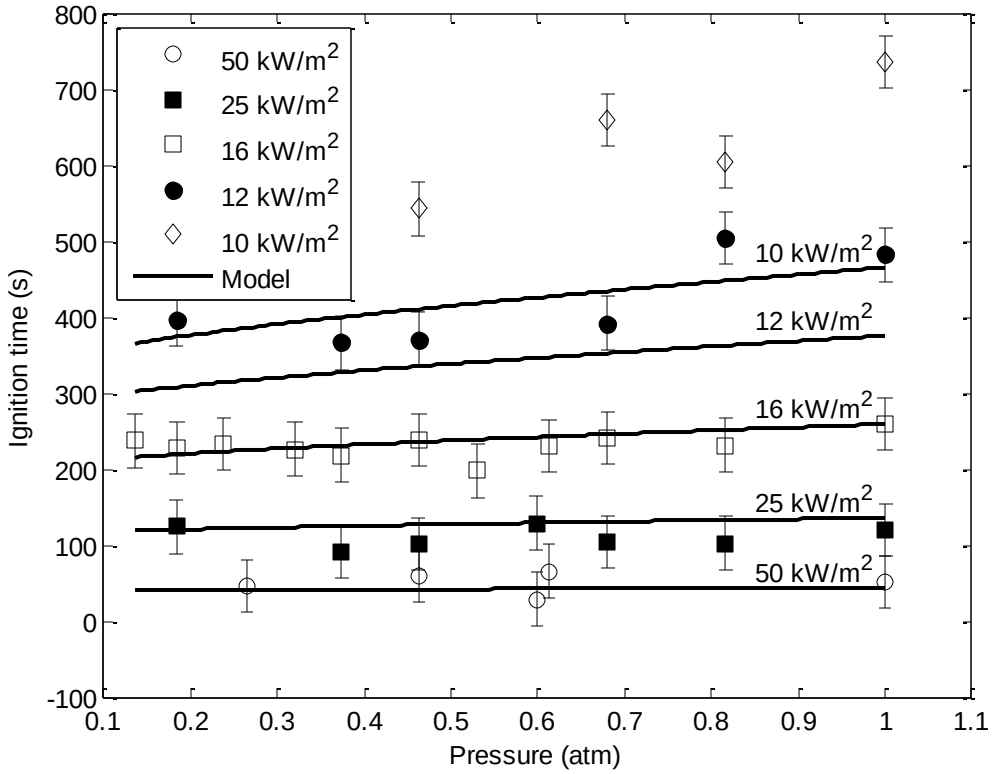

Figure 4.9 Comparison of theoretical analysis for time to ignition with the experimental results.

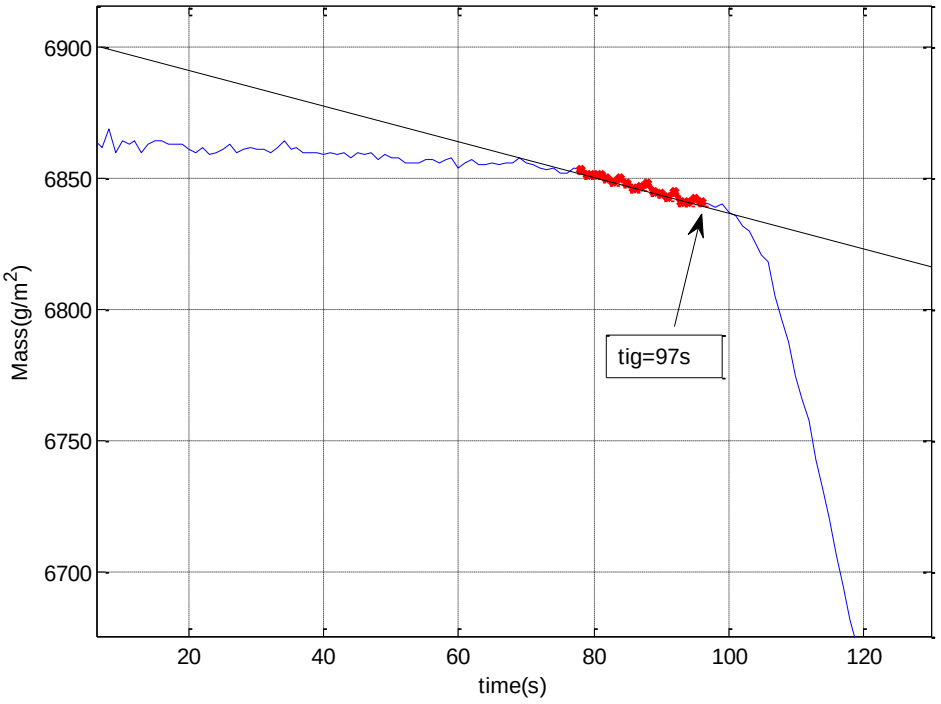

Figure 4.10 The method for calculating the mass flux at ignition. The mass flux was taken to be the slope of the mass loss data for 20 seconds before ignition.

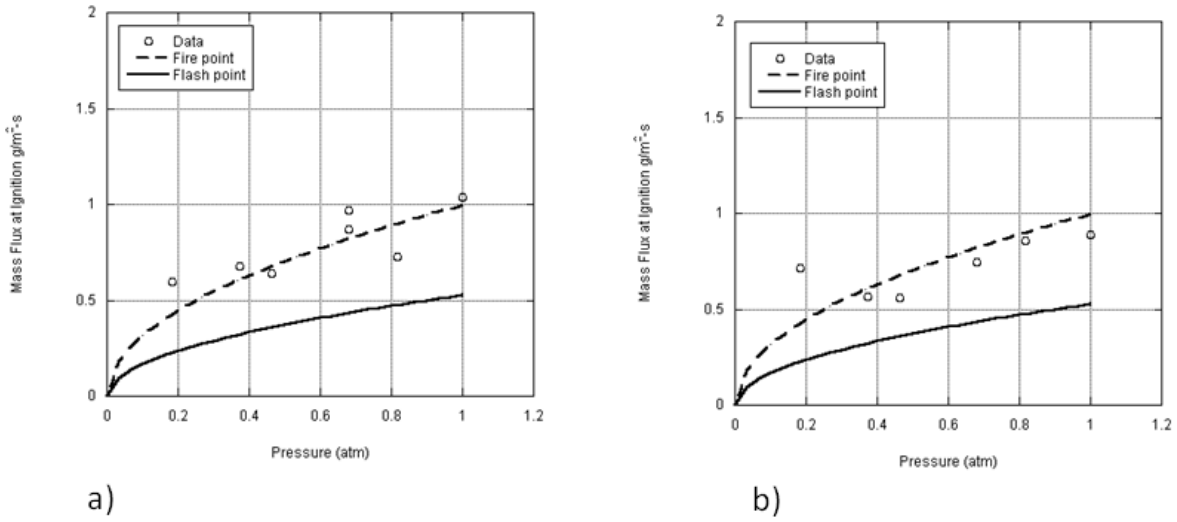

Figure 4.11 Mass flux at ignition calculated using the average mass flux for 20 seconds before ignition.

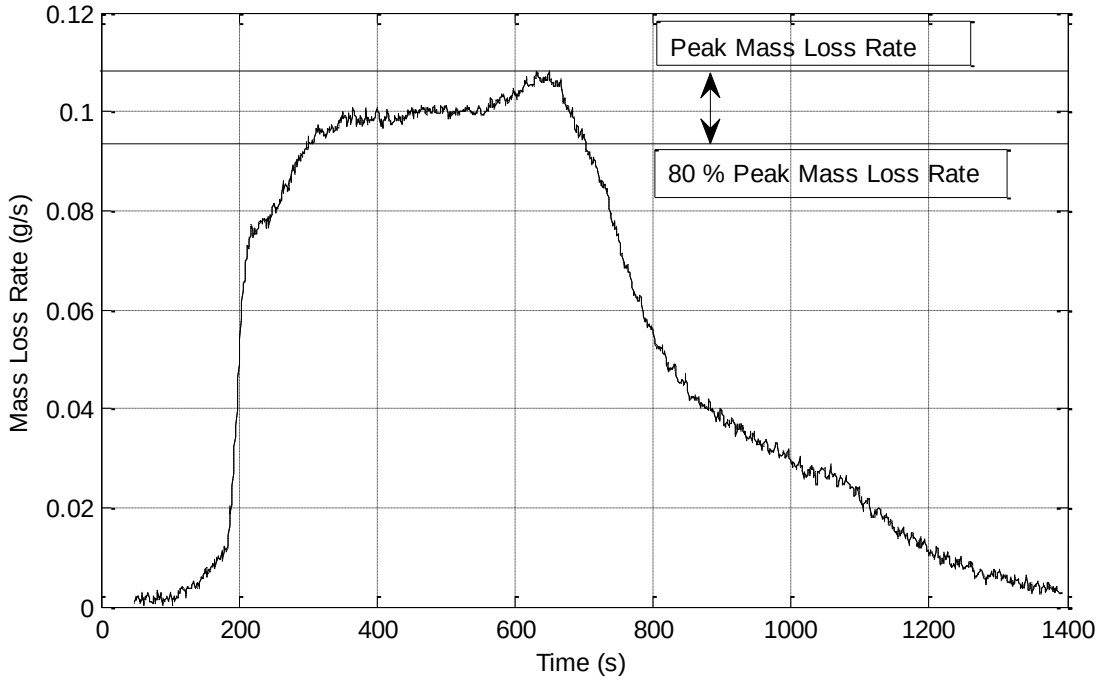

Figure 4.12 Time interval used to calculate the average mass loss rate.

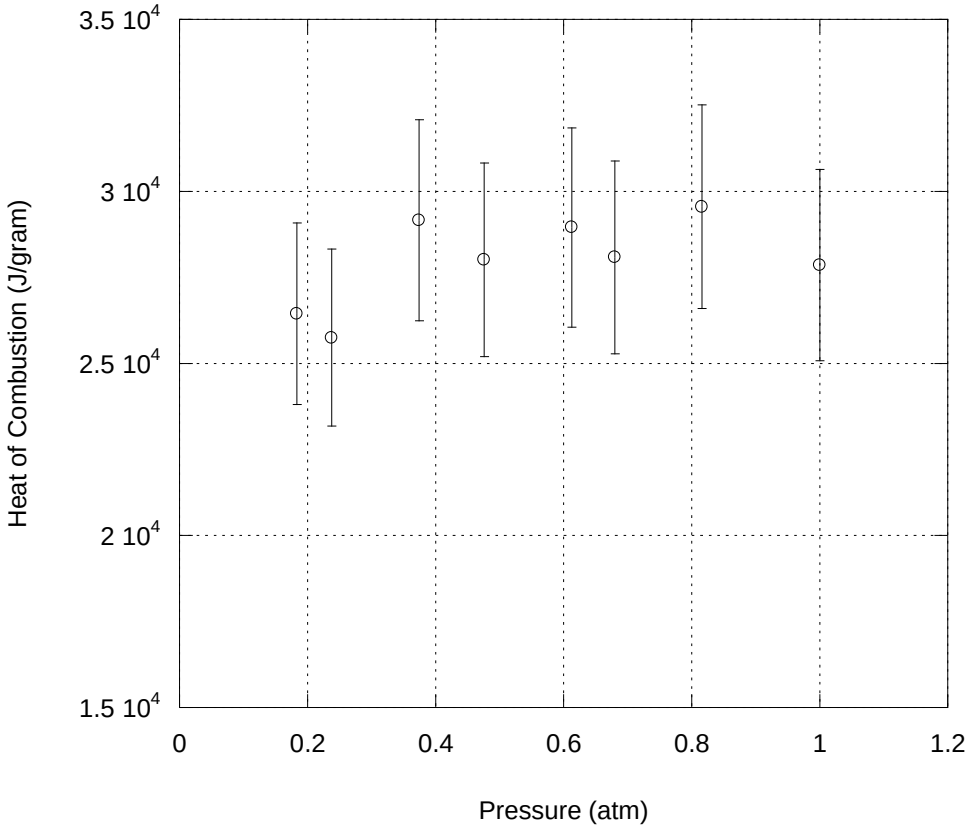

Figure 4.13 Effective heat of combustion calculated using oxygen consumption calorimetry..

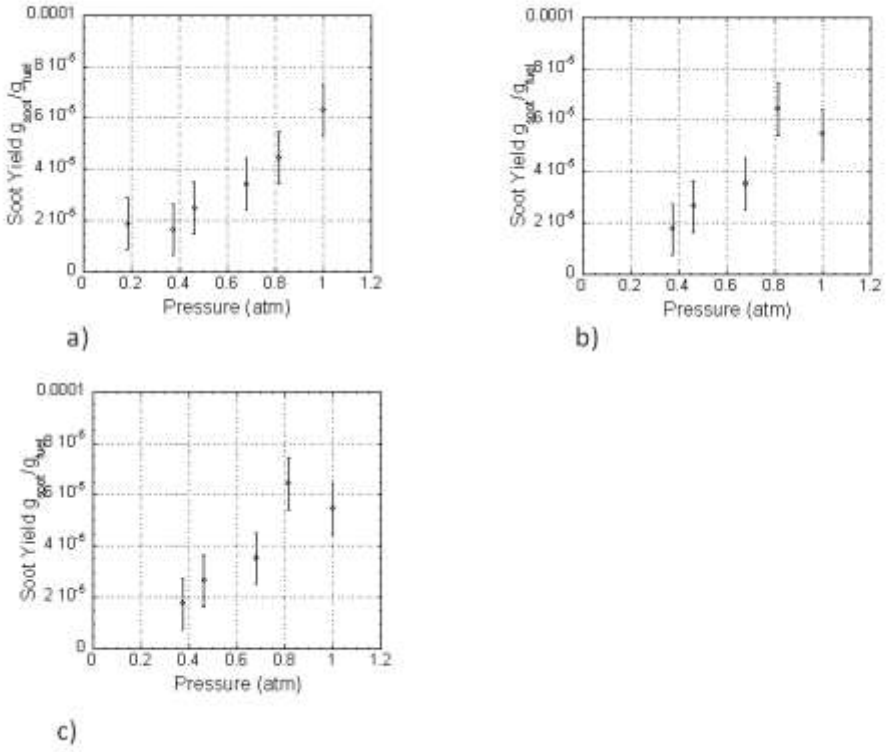

Figure 4.14 Soot yields versus total pressure for a)10 kW/m^2, b) 12 kW/m^2, and c)16 kW/m^2 external heat flux. There is a clear decrease of soot yield at lower pressure for all cases.

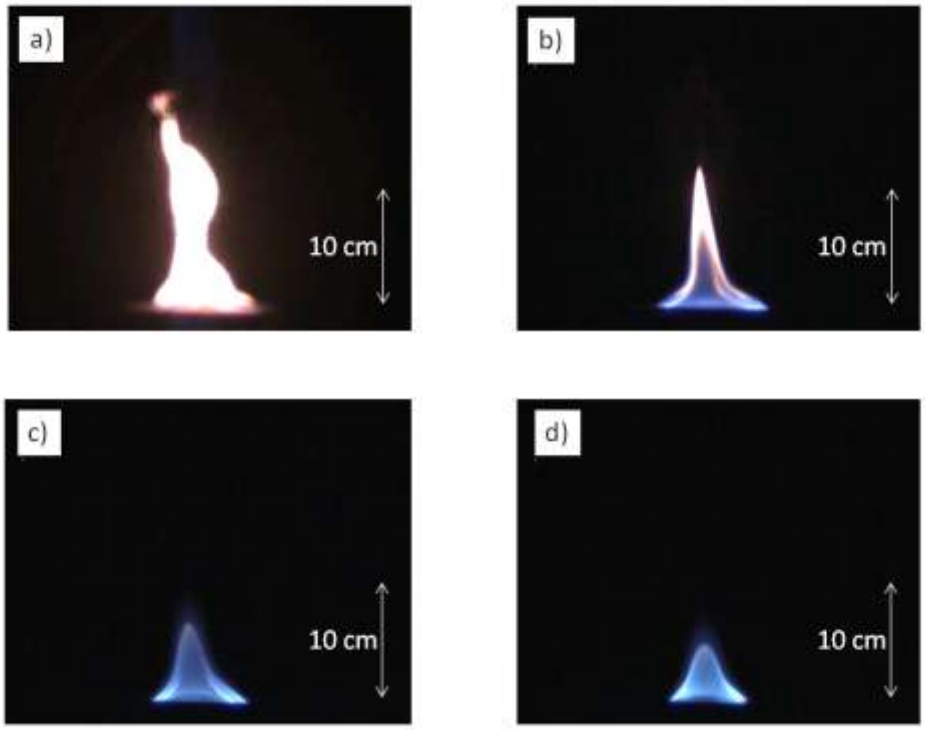

Figure 4.15 Flame profiles for a) 1 atm, b) 0.68 atm, c) 0.47 tm and d) 0.18 atm. The flame changes color and decreases in size with the decrease in the total pressure.

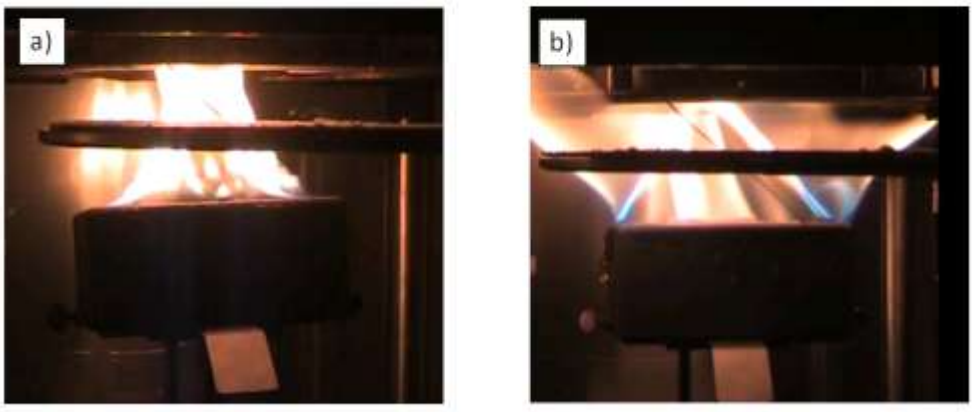

Figure 4.16 Flame profiles at a) 1 atm and b) 0.18 atm show a distinct reduction in the buoyancy.

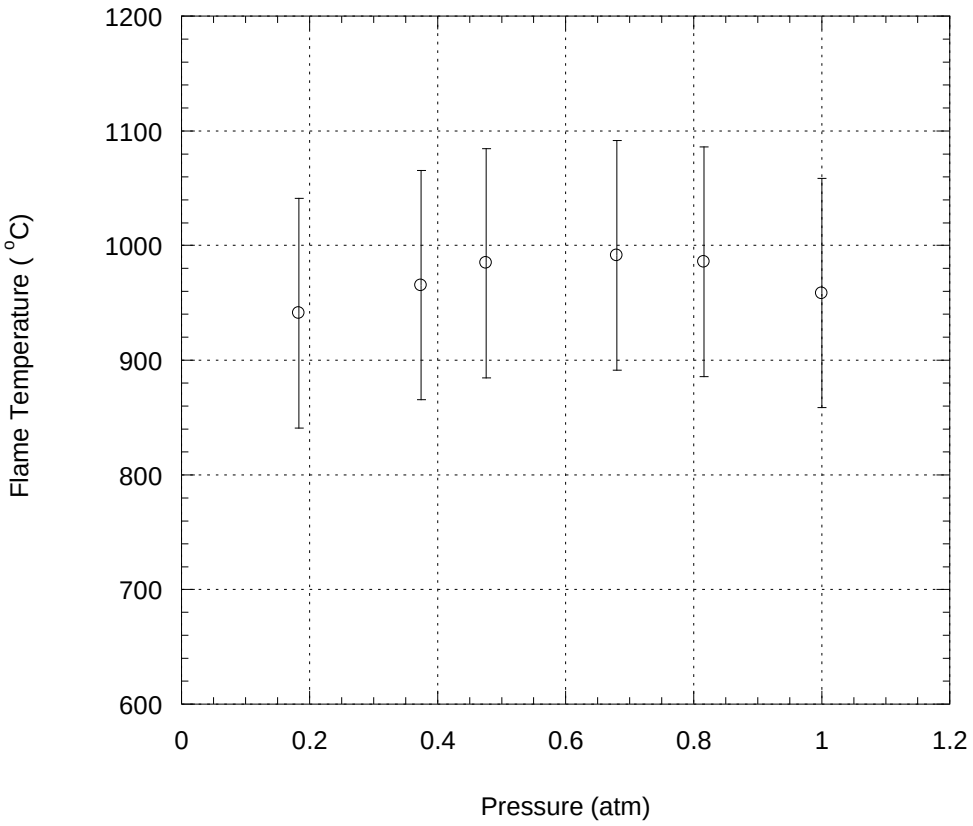

Figure 4.17 Average flame temperature plotted versus total pressure.

Chapter 5

Conclusion

The flammability of a material can be describe by how easily it ignites, how fast does the flame spread once its ignited, and how intense is the fire. The intensity of the fire can be quantified by measuring the mass loss rate, or by measuring the amount of oxygen consumed. In order to fully understand how flammable a material is, the environment in which it is used has to be considered. The variation of pressure with altitude plays an important role in the behavior of the fire and therefore cannot be ignored.

The effect of pressure on the mass loss rate during combustion is discussed in chapter 3. The pressure effect on convective heat transfer from the flame can be deduced from the Grashof number. It was shown that the convective heat transfer coefficient varies as the square root of power with pressure. The literature review suggested that the radiative heat transfer was controlled by the soot volume fractions. de Ris (2000) deduced that the soot volume fraction scaled a pressure squared [23]. The results for the soot yield, in chapter 4, suggested a linear relationship for the tests performed. The linear relation was used in the analytical model and the results yielded a good agreement with the experimental results.

Tests were also performed in a reduced oxygen environment at different pressures. It was observed that the intensity of the fire was lower at lower oxygen concentration. This is consistent with the fact that the flame temperature is lower at lower oxygen concentration as seen in Eq. 3.22a. The effect of low oxygen at 0.18 atm was shown to have little effect on the mass loss rate, but the samples were not able to ignite at 15 % oxygen or below. This is in contrast to the conditions at ambient as the sample was able to ignite at 13 % of oxygen.

Overall the theoretical analysis was able to predict the behavior of the fire at reduced pressure and oxygen concentrations. It was shown that a fire at low pressure will burn with a lower intensity and that could in effect give the pilots enough time to land the airplane. Although the fire was more controllable at high altitude, the airplane has to land eventually, which might cause the fire to intensify again. This has not been considered in this study but might warrant some consideration in the future. Given all of that, if depressurization is used in combination with nitrogen to suppress the fire, the amount of nitrogen needed might be lower at high altitude.

References

[1] Junior Worldmark Encyclopedia of World Cities. 2000. *Ecyclopedia.com*. Dec. 5, 2011. <Encyclopedia.com>

[2] Federal Aviation Administration. *In-Flight Fires,* Advisory Circular 120-80, U.S. Department of Transportation, 2004.

[3] National Transportation safety board. *Inflight Cargo fire*, Aircraft Accident Report, NTSB/AAR-07/07. 2007

[4] Tewarson, A., *Nonmetallic Material Flammability in Oxygen Enriched Atmospheres*, Journal of Fire Science, Vol. 18, 2000, p. 183-214.

[5] Frey, A.E., and T'ien, J.S. *Near-Limit Flame Spread over Paper Samples*, Combustion and Flame, 26, 1976, pp. 257-267.

[6] McAlevy, R., and Magee, R.S., *The Mechanisms of Flame Spreading over the Surface of Igniting Condensed-Phase Materials*, Proceedings of the Combustion Institute, Vol. 12, 1969, pp. 215-227.

[7] West, John B., *Fire Hazard in Oxygen-Enriched Atmospheres at Low Barometric Pressures*: Aviation, Space, and Envir. Med., vol. 68, 1997, p. 159-163.

[8] Nakamura, Y., Yoshimura, N., Ito, H., Azumaya, K., and Fujita, O. *Flame Spread over Electric Wire in Sub-Atmospheric Pressure, Proceedings of the Combustion Institute,* Vol. 32, 2009

[9] Roditcheva, O.V., Bai, X.S., *Pressure Effect on Soot Formation in Turbulent Diffusion Flames*, Chemosphere, 2001, Vol. 42, No. 5-7, p. 811-821.

[10] Beltrame, A., Porschnev, P., Merchan-Merchan, W., Saveliev, A., Fridman, A., Kennedy, L.A., Pertrova, O., Zhdanok, S., Amouri, F. and Charon, O., *Soot and NO Formation in Methane–Oxygen Enriched Diffusion Flames*, Combustion and Flame, Vol. 124, Issues 1-2, Jan. 2001, p. 295-310

[11] Tewarson, A. Lee, J.L. Pion, R.F., *The influence of oxygen concentration on fuel parameters for fire modelling*, Proceedings of the Combustion Institute 18 (1981) 563–570.

[12] McAllister, S., Fernandez-Pello, C., Urban, D., Ruff, G., *The combined effect of pressure and oxygen concentration on piloted ignition of a solid combustible,* Combust. Flame 157 (9) (2010) p.1753–1759.

[13] Goldmeer, Jeffrey Scott, *Extinguishment of a Diffusion Flame Over a PMMA Cylinder by Depressurization in Reduced-Gravity,* Glenn Research Center, E-10552; NAS 1.26:198550; NASA-CR-19855

[14] ASTM E 1354, *Standard Test Method for Heat and Visible Smoke Release Rates for Materials and Products Using Oxygen Depletion,* American Society for Testing and Materials, Philadelphia PA.

[15] Thornton, W. M., *The Relation of Oxygen to the Heat of Combustion of Organic Compounds*, *Philos. Mag., Ser. 6* 33, 1917, p. 196-203.

[16] Huggett, C., *Estimation of Rate of Heat Release by Means of Oxygen Consumption Measurements*, *Fire Mater.* 4,1980, p.61-65

[17] Babrauskas, V., and Grayson, S.J., eds., *Heat Release in Fires*, Elsevier Applied Science Publishers, London, 1992.

[18] Quintiere, J. G., *Fundamentals of Fire Phenomena,* John Wiley & Sons, Ltd., West Sussex, England, 1993. Wiley-Interscience. New York.

[19] Ozisik, M.N., *Heat Conduction*, 2nd Edition, John Wiley & Sons Inc.,New York, 1993

[20] Tewarson, A., *Generation of Heat and Chemical Compounds in Fires,* SFPE Handbook of Fire Protection Engineering, 3rd ed., National Fire Protection Association, 2002, Section 3, Chapter 4

[21] Yuen, W.W. & Tien, C.L., *A Simple calculation scheme for the luminous-flame emissivity*. Sixteenth Sym. (Int.) on Combustion, The Combustion Institute, Pittsburg, PA, 1982, p.1481-1487.

[22] Heskestad, G., *Luminous height of turbulent flames*, Fire Safety Journal, Volume 5, Issue 2, 1983, p. 103-108

[23] Incropera, F.P. and DeWitt, D. P., *Fundamentals of Heat and Mass Transfer*, 4th Ed., John Wiley and Sons, NY, 1996.

[24] *de Ris* J, Wu PK, Heskestad G. *Radiation fire modeling*. Proc Combust Inst 2000;28:2751–9

[25] *Tewarson*, A. and Pion, R, *Flammability of plastics – I. Burning Intensity,* Combustion and. Flame, 26, 1976, p. 85 – 103.

[26] Rhodes, B.T. and Quintiere, J.G., *Burning rate and flame heat flux for PMMA in a cone calorimeter*, Fire Safety Journal, Volume 26, Issue 3, 1996, Pages 221-240

[27] Stoliarov, S.I. and Walters R.N., *Determination of the heats of gasification of polymers using differential scanning calorimetry,* Polymer Degradation and Stability, Volume 93, Issue 2, 2008, Pages 422-427

[28] Babrauskas, V., *Ignition Handbook,* Fire Science Publishers/Society of Fire Protection Engineers, Issaquah WA, 2003.

[29] Drysdale, D., in *An Introduction to Fire Dynamics*, Third Edition, John Wiley & Sons, Ltd, Chichester, UK, 2011.

[30] Fereres, S., Lautenberger, C., Fernandez-Pello, C., Urban, D.L., Ruff, G.A. *Mass flux at ignition in reduced pressure environments,* Combustion and Flame, Volume 158, Issue 7, 2011, Pages 1301-1306

[31] Walters, R.N., Hackett, S.M.,Lyon, R.E. Heat of combustion of high temperature polymers, DOT/FAA/AR-TN97/8

[32] Liu, Xin and Quintiere, J.G*., Flammability Properties of Clay-Nylon Nanocomposites*, DOT/FAA/AR-07/29

[33] Kashiwagi, T., Inaba, A. and Brown, J.E., *Differences In Pmma Degradation Characteristics And Their Effects On Its Fire Properties*. Fire Safety Science 1: 483-493. doi:10.3801/IAFSS.FSS.1-483, 1986.